An efficient and robust integration scheme for the equations of motion of the multiconfiguration time-dependent Hartree (MCTDH) method

ARTICLE *in* ZEITSCHRIFT FÜR PHYSIK D · JANUARY 1997

DOI: 10.1007/s004600050342

2 AUTHORS, INCLUDING:

Hans-Dieter Meyer
Universität Heidelberg
245 PUBLICATIONS **9,779** CITATIONS

Z. Phys. D 42, 113–129 (1997)

ZEITSCHRIFT
FÜR PHYSIK D

An efficient and robust integration scheme for the equations of motion of the multiconfiguration time-dependent Hartree (MCTDH) method

M.H. Beck, H.-D. Meyer

Theoretische Chemie, Physikalisch-Chemisches Institut, Im Neuenheimer Feld 253, D-69120 Heidelberg, Germany

Received: 30 June 1997 / Final version: 7 August 1997

Abstract. An efficient and robust integration scheme tailored to the equations of motion of the multiconfiguration time-dependent Hartree (MCTDH) method is presented. An error estimation allows the automatical adjustment of the step size and hence controls the integration error. The integration scheme decouples the MCTDH equations of motion into several disjoined subsystems, of which one determines the time evolution of the MCTDH-coefficients. While the conventional MCTDH equations are non-linear, the working equation for the MCTDH-coefficients becomes linear in the present integration scheme. To investigate the integrator's performance it is applied to the photodissociation process of methyl iodide. The results of the novel integration scheme are in perfect agreement to those obtained by solving the MCTDH working equations conventionally. The computation time, however, is reduced by a factor of about ten when the new integration scheme is used to propagate large systems.

PACS: 02.70.Ns, 31.70.Hq

I Introduction

The time-dependent quantum mechanical treatment of molecular dynamics, which numerically solves the time-dependent Schrödinger equation, has gained rapidly increasing interest and importance during the last fifteen years. Although for time-independent Hamiltonians this approach is formally equivalent to solving the time-independent Schrödinger equation, it offers a number of advantages. While in the time-independent framework one has to solve an eigenvalue problem, one is faced in the time-dependent picture with an initial value problem, which is mathematically simpler. Moreover, time-dependent methods can handle systems that involve continuum states (e. g. chemical reactions or photodissociation processes) very easily. Employing a time-independent procedure in this case, the wave function becomes a continuum function subject to complicated scattering boundary conditions. In contrast, turning to a time-dependent treatment the wave function remains square integrable, and there is virtually no difference between propagating a wave-packet that is a superposition of bound or of continuum states. Besides these rather technical advantages, time-dependent schemes offer a deeper insight into the dynamics, and hence lead to a better understanding of the physical process under investigation. Finally, if the Hamiltonian is itself time-dependent, one must of course adopt the time-dependent framework.

Apart from the development of the computational facilities there has been a considerable progress over the last fifteen years in improving the algorithms for solving the time-dependent Schrödinger equation numerically exactly. Powerful integrators [1,2] and representation schemes [3–6] are now available. Nevertheless, a numerically exact quantum mechanical treatment of the wave-packet dynamics is in general restricted to three- or four-dimensional systems due to the exponential increase of numerical effort and main memory with the number of degrees of freedom.

To overcome these limitations it is essential to develop approximate schemes for calculating wave-packet dynamics which require less computational resources. Examples for such methods are the Gaussian wave-packet method of Heller [7] or a mixed classical/quantal description [8,9]. Further we mention the semiclassical initial value representation (IVR). Very recently this method has been used to study the dynamics of a system with remarkable fifteen degrees of freedom (see [10] and references therein). A purely quantal approximation to the time-dependent Schrödinger equation is the time-dependent Hartree (TDH) method, also known as time-dependent self-consistent field (TDSCF) [11, 12]. Very large systems have been studied employing the TDSCF method [13–15]. All these schemes reduce the computational effort considerably. However, only for selected cases is their accuracy sufficient for a quantative analysis.

In the present work we focus on the multiconfiguration time-dependent Hartree (MCTDH) method [16–19]. This approximate scheme is capable of treating multidimensional dynamics efficiently and with controllable accuracy. Its reliability and efficiency is confirmed through a variety of calculations. The MCTDH scheme has successfully been applied to the photodissociation processes of NOCl [17], NO_2 [20], CH_3I [21, 22] and ICN [23], and to the vibrational predis-

sociation dynamics of Cl_2Ne [24]. Molecule surface scattering is another field of interest. Rotational excitation via molecule/surface scattering has been investigated for the systems H_2/LiF [25] and N_2/LiF [26], dissociation was studied for a H_2/metal system [27] and for CH_4/Ni [28], and photodissociation has been analyzed for CH_3I/MgO [29, 30]. MCTDH has also been used to study the hydrogen exchange reaction $H + H_2 \rightarrow H_2 + H$ [31] and to explore the absorption spectrum of pyrazine [32]. The latter work is particularly remarkable because there it was possible to accurately account for the motion of 14 vibrational modes on two coupled electronic potential energy surfaces.

Despite the various successful calculations performed so far, the MCTDH algorithm has to be improved further in order to be applicable to larger polyatomic systems. The MCTDH equations of motion form a set of coupled nonlinear ordinary differential equations of first order. Part of the difficulty in applying the MCTDH scheme to large molecules results from the fact that the wave function contains parts that are highly oscillatory in time. This enforces small integration steps and hence a large number of evaluations of the differential equations. To overcome this problem we introduce in this work an integration scheme to solve the MCTDH equations of motion that is both efficient and robust, and simultaneously allows a precise control of the integration error. The integration scheme, which defines a second order method with variable step size, is easy to handle and leads to a considerable speed-up of the MCTDH method, especially for systems with many degrees of freedom. To demonstrate the integrator's efficiency and practicability, it is applied to the photodissociation process of methyl iodide.

The paper is organized as follows. In Sect. II we review the basic equations of the MCTDH method and discuss the computational effort required to evaluate the MCTDH equations of motion. The efficient and robust integration scheme for the MCTDH working equations is then presented in Sect. III. In Sect. IV our calculations on the photodissociation process of CH_3I are described and their results are discussed. Section V gives a short summary. Finally, in Appendix A the error estimation of the Lanczos integrator is critically examined and an improved one is proposed. Throughout this paper a unit system is used where $\hbar = 1$.

II The MCTDH method

A The MCTDH equations of motion

The derivation of the MCTDH equations of motion has been described in detail in preceding papers [16–18], so only an outline will be given here.

In the MCTDH scheme the wave function Ψ describing the molecular dynamics of a system with f degrees of freedom is a time-dependent multiconfigurational function of the nuclear coordinates $Q_1, \ldots, Q_f$:

$$\Psi(Q_1, \ldots, Q_f, t) = \sum_{j_1=1}^{n_1} \cdots \sum_{j_f=1}^{n_f} A_{j_1 \ldots j_f}(t) \times \prod_{\kappa=1}^{f} \varphi_{j_\kappa}^{(\kappa)}(Q_\kappa, t)\,, \tag{1}$$

where the $A_{j_1 \ldots j_f}$ denote the MCTDH expansion coefficients, and the $\varphi_{j_\kappa}^{(\kappa)}$ are the n_κ expansion functions for each degree of freedom κ, known as *single-particle functions*.

Since both the MCTDH-coefficients and the single-particle functions are time-dependent, the MCTDH wave function (1) contains redundancies which are removed by imposing the constraints

$$\langle \varphi_j^{(\kappa)}(0) \mid \varphi_l^{(\kappa)}(0) \rangle = \delta_{jl} \tag{2}$$

and either

$$\langle \varphi_j^{(\kappa)}(t) \mid \dot{\varphi}_l^{(\kappa)}(t) \rangle = 0 \tag{3}$$

or

$$\langle \varphi_j^{(\kappa)}(t) \mid \dot{\varphi}_l^{(\kappa)}(t) \rangle = -\mathrm{i}\, \langle \varphi_j^{(\kappa)}(t) \mid h^{(\kappa)} \mid \varphi_l^{(\kappa)}(t) \rangle \tag{4}$$

on the single-particle functions. Here the so-called *single-particle operator* $h^{(\kappa)}$ is a hermitian, but otherwise arbitrary, operator acting exclusively on the κth degree of freedom. The single-particle operators serve to partition the Hamiltonian H into a separable and a residual part, i. e.

$$H = \sum_{\kappa=1}^{f} h^{(\kappa)} + H_R\,. \tag{5}$$

The constraints (2) and (3) or (4) imply that the single-particle functions remain orthonormal for all times.

Before presenting the MCTDH working equations we simplify the notation by establishing the composite index J and the configurations Φ_J by

$$\Phi_J = \prod_{\kappa=1}^{f} \varphi_{j_\kappa}^{(\kappa)}\,. \tag{6}$$

Further we introduce

$$P^{(\kappa)} = \sum_{j=1}^{n_\kappa} \mid \varphi_j^{(\kappa)} \rangle \langle \varphi_j^{(\kappa)} \mid \tag{7}$$

as the projector on the space spanned by the single-particle functions for the κth degree of freedom, and the *single-hole functions* $\Psi_l^{(\kappa)}$ as the linear combination of Hartree products of $(f-1)$ single-particle functions that do not contain the coordinate Q_κ:

$$\Psi_l^{(\kappa)} = \sum_{j_1} \cdots \sum_{j_{\kappa-1}} \sum_{j_{\kappa+1}} \cdots \sum_{j_f} A_{j_1 \ldots j_{\kappa-1} l j_{\kappa+1} \ldots j_f} \times \varphi_{j_1}^{(1)} \ldots \varphi_{j_{\kappa-1}}^{(\kappa-1)} \varphi_{j_{\kappa+1}}^{(\kappa+1)} \ldots \varphi_{j_f}^{(f)}\,. \tag{8}$$

The single-hole functions enable us to define the mean-fields

$$\langle H_R \rangle_{jl}^{(\kappa)} = \langle \Psi_j^{(\kappa)} \mid H_R \mid \Psi_l^{(\kappa)} \rangle \tag{9}$$

and density matrices

$$\rho_{jl}^{(\kappa)} = \langle \Psi_j^{(\kappa)} \mid \Psi_l^{(\kappa)} \rangle = \sum_{j_1} \cdots \sum_{j_{\kappa-1}} \sum_{j_{\kappa+1}} \cdots \sum_{j_f} A^*_{j_1 \ldots j_{\kappa-1} j j_{\kappa+1} \ldots j_f} \times A_{j_1 \ldots j_{\kappa-1} l j_{\kappa+1} \ldots j_f}\,, \tag{10}$$

given in the basis of the single-particle functions. Note that $\langle H_R \rangle_{jl}^{(\kappa)}$ is an operator acting on the κth degree of freedom

and that the trace of $\boldsymbol{\rho}^{(\kappa)}$ equals $\|\Psi\|^2$ due to the orthonormality of the single-particle functions. Finally, we adopt the vector notation

$$\boldsymbol{\varphi}^{(\kappa)} = \left(\varphi_1^{(\kappa)}, \ldots, \varphi_{n_\kappa}^{(\kappa)}\right)^T \tag{11}$$

for the n_κ single-particle functions used to represent mode κ.

The equations of motion are then derived by variationally optimizing the MCTDH wave function (1), employing the Dirac-Frenkel variational principle [11, 33]

$$\langle \delta\Psi \mid H - \mathrm{i}\,\partial_t \mid \Psi\rangle = 0\,, \tag{12}$$

leading to

$$\mathrm{i}\dot{A}_J = \sum_L \langle \Phi_J \mid H \mid \Phi_L\rangle A_L\,, \tag{13}$$

$$\begin{aligned}\mathrm{i}\,\dot{\boldsymbol{\varphi}}^{(\kappa)} = \left(1 - P^{(\kappa)}\right) \Bigg(& h^{(\kappa)}\,\mathbf{1}_{n_\kappa} \\ & + \left(\boldsymbol{\rho}^{(\kappa)}\right)^{-1} \langle \mathbf{H_R}\rangle^{(\kappa)} \Bigg) \boldsymbol{\varphi}^{(\kappa)}\,,\end{aligned} \tag{14}$$

when the constraints (2) and (3) are used, or

$$\mathrm{i}\dot{A}_J = \sum_L \langle \Phi_J \mid H_R \mid \Phi_L\rangle A_L\,, \tag{15}$$

$$\begin{aligned}\mathrm{i}\,\dot{\boldsymbol{\varphi}}^{(\kappa)} = \Bigg(& h^{(\kappa)}\,\mathbf{1}_{n_\kappa} + \left(1 - P^{(\kappa)}\right) \\ & \times \left(\boldsymbol{\rho}^{(\kappa)}\right)^{-1} \langle \mathbf{H_R}\rangle^{(\kappa)} \Bigg) \boldsymbol{\varphi}^{(\kappa)}\,,\end{aligned} \tag{16}$$

if the constraints (2) and (4) are applied. Here $\mathbf{1}_{n_\kappa}$ denotes the $n_\kappa \times n_\kappa$ unit matrix. Note that the MCTDH equations of motion form a system of coupled non-linear ordinary differential equations of first order.

Compared to (15), the working equation (13) has the disadvantage that the full Hamiltonian H instead of the residual Hamiltonian H_R is employed in the propagation of the MCTDH-coefficients, which is computationally more expensive. For example, in case of the 4-mode model for the pyrazine molecule [32] a calculation employing (13) and (14) is 8% slower compared to one using (15) and (16). The use of (14) however means that the motion of the single-particle functions is minimized, because the projector exclusively allows motions in directions perpendicular to the space spanned by the single-particle functions. The integration scheme to be described below is more efficient when the single-particle functions move as little as possible. For that reason we choose in the following the constraints (2) and (3) and thus use the equations of motion (13) and (14).

The MCTDH-algorithm can also be applied to systems where more than one electronic state is included. One possibility to accomplish this is to choose one extra degree of freedom, the fth say, to represent the electronic manifold. The variable Q_f then labels the electronic states, taking only discrete values $Q_f = 1, 2, \ldots, \sigma$, where σ is the number of states under consideration. The number of single-particle functions for such an electronic mode is set to the number of states, i. e. $n_f = \sigma$. The equations of motion (13) and (14) remain unchanged, treating nuclear and electronic modes on the same footings. This we call the *single-set* formulation since only one set of single-particle functions is used for all the electronic states.

Contrary to this, the *multi-set* formulation employs different sets of single-particle functions for each electronic state. In this formulation the Hamiltonian H is expanded in the set $\{\mid \alpha\rangle\}$ of electronic states:

$$H = \sum_{\alpha,\beta=1}^{\sigma} \mid \alpha\rangle\, H^{(\alpha\beta)}\, \langle \beta \mid\ . \tag{17}$$

Using again the constraints (2) and (3), the equations of motion read

$$\mathrm{i}\dot{A}_J^{(\beta)} = \sum_{\alpha=1}^{\sigma} \sum_L \langle \Phi_J^{(\beta)} \mid H^{(\beta\alpha)} \mid \Phi_L^{(\alpha)}\rangle\, A_L^{(\alpha)}\,, \tag{18}$$

$$\begin{aligned}\mathrm{i}\,\dot{\boldsymbol{\varphi}}^{(\beta,\kappa)} = \left(1 - P^{(\beta,\kappa)}\right) \Bigg(& h^{(\beta,\kappa)}\,\mathbf{1}_{n_\kappa} \\ & + \left(\boldsymbol{\rho}^{(\beta,\kappa)}\right)^{-1} \sum_{\alpha=1}^{\sigma} \langle \mathbf{H_R}\rangle^{(\beta\alpha,\kappa)} \Bigg) \boldsymbol{\varphi}^{(\alpha,\kappa)}\,,\end{aligned} \tag{19}$$

with mean-fields

$$\langle H_R\rangle_{jl}^{(\beta\alpha,\kappa)} = \langle \Psi_j^{(\beta,\kappa)} \mid H_R^{(\beta\alpha)} \mid \Psi_l^{(\alpha,\kappa)}\rangle\,. \tag{20}$$

The superscripts α and β denote to which electronic state the functions and operators belong. A derivation of these equations is given in [29] and [32].

We close this section in emphasizing that the MCTDH equations conserve the norm and, for time-independent Hamiltonians, the total energy. This follows directly from the variational principle. Moreover, the MCTDH wave function converges towards the numerically exact one with increasing numbers of single-particle functions.

B Numerical evaluation

The MCTDH equations of motion as derived in the preceding section II.A have to be slightly modified for numerical reasons.

The first change concerns the projection operator $P^{(\kappa)}$. This projector ensures the constraints (2) and (3) and preserves the orthonormality of the single-particle functions during the propagation. If the single-particle functions however become non-orthonormal due to inaccuracies of the integration, $P^{(\kappa)}$ ceases to be a projector, and even an exact solution of (14) will then further destroy the orthonormality. A cure to this numerical problem is to define the projector as

$$P^{(\kappa)} = \sum_{j,l=1}^{n_\kappa} \mid \varphi_j^{(\kappa)}\rangle \left(\left(\boldsymbol{\mathcal{O}}^{(\kappa)}\right)^{-1}\right)_{jl} \langle \varphi_l^{(\kappa)} \mid \tag{21}$$

where $\mathcal{O}_{jl}^{(\kappa)} = \langle \varphi_j^{(\kappa)} \mid \varphi_l^{(\kappa)}\rangle$ denotes the overlap matrix of the single-particle functions. Equation (21) defines an orthonormal projector as long as the single-particle functions are linearly independent; their orthonormality is not required.

The second modification refers to the density matrix $\boldsymbol{\rho}^{(\kappa)}$. The eigenvalues, called *natural populations*, of this hermitian and positive semi-definite matrix characterize the importance of the corresponding eigenfunctions or *natural orbitals*. If there is a natural orbital (i. e. a linear combination

of the single-particle functions) that does not contribute to the MCTDH wave function, the density matrix will become singular and may be replaced by a regularized one such as

$$\boldsymbol{\rho}^{(\kappa)}_{\rm reg} = \boldsymbol{\rho}^{(\kappa)} + \varepsilon \exp\left(-\boldsymbol{\rho}^{(\kappa)}/\varepsilon\right) , \tag{22}$$

with ε being a small number. (In the calculations depicted later we have used $\varepsilon = 10^{-8}$.) When complex absorbing potentials [34–41] are employed, the wave function vanishes for large times. To compensate for this, ε is weighted with the squared norm of the wave function, i. e. $\varepsilon \to \varepsilon\,{\rm tr}(\boldsymbol{\rho}^{(\kappa)})$. Note that the regularization changes only the time evolution of those natural orbitals that are very weakly populated; the time evolution of the natural orbitals important for the description of the wave function remains unchanged.

Thirdly, for the MCTDH algorithm to be efficient one has to avoid the direct evaluation of the Hamiltonian matrix elements $\langle \Phi_J \mid H \mid \Phi_L \rangle$ and mean-fields $\langle H_R \rangle^{(\kappa)}_{jl} = \langle \Psi^{(\kappa)}_j \mid H_R \mid \Psi^{(\kappa)}_l \rangle$, since this would require f-fold and $(f-1)$-fold integrations, respectively. These multidimensional integrations can be circumvented if the residual Hamiltonian H_R is written as a sum of products of single-particle operators,

$$H_R = \sum_{r=1}^{s} c_r \prod_{\kappa=1}^{f} h^{(\kappa)}_r , \tag{23}$$

with expansion coefficients c_r. The kinetic energy operators are normally of the required form (23). If a potential has not the necessary structure it must be fit to the product form. A convenient and systematic approach to obtain such a representation has recently been developed [42].

Using (23) the matrix elements can be expanded as

$$\begin{aligned}\langle \Phi_J \mid H \mid \Phi_L \rangle = &\sum_{\kappa=1}^{f} \langle \varphi^{(\kappa)}_{j_\kappa} \mid h^{(\kappa)} \mid \varphi^{(\kappa)}_{l_\kappa} \rangle \\ &+ \sum_{r=1}^{s} c_r \prod_{\kappa=1}^{f} \langle \varphi^{(\kappa)}_{j_\kappa} \mid h^{(\kappa)}_r \mid \varphi^{(\kappa)}_{l_\kappa} \rangle .\end{aligned} \tag{24}$$

Again the $h^{(\kappa)}$ and $h^{(\kappa)}_r$ denote the single-particle operators building up the separable and the residual part of the Hamiltonian, respectively. The mean-field operators now read

$$\langle H_R \rangle^{(\kappa)}_{jl} = \sum_{r=1}^{s} \boldsymbol{\mathcal{H}}^{(\kappa)}_{rjl} h^{(\kappa)}_r , \tag{25}$$

where the so-called *mean-field matrix* $\boldsymbol{\mathcal{H}}^{(\kappa)}_r$ has elements

$$\begin{aligned}\boldsymbol{\mathcal{H}}^{(\kappa)}_{rjl} = c_r \sum_{j_1} \dots \sum_{j_f} & A^*_{j_1 \dots j_{\kappa-1} j j_{\kappa+1} \dots j_f} \\ &\times \Bigg(\sum_{l_1} \langle \varphi^{(1)}_{j_1} \mid h^{(1)}_r \mid \varphi^{(1)}_{l_1} \rangle \dots \\ &\times \Bigg(\sum_{l_f} \langle \varphi^{(f)}_{j_f} \mid h^{(f)}_r \mid \varphi^{(f)}_{l_f} \rangle \\ &\times A_{l_1 \dots l_{\kappa-1} l l_{\kappa+1} \dots l_f} \Bigg) \Bigg) .\end{aligned} \tag{26}$$

Note that "…" does not contain j_κ and l_κ. The time-derivative (13) of the MCTDH-coefficients is obtained by

$$\begin{aligned}{\rm i}\dot{A}_J = &\sum_{\kappa=1}^{f} \sum_{l_1} \dots \sum_{l_f} \langle \varphi^{(\kappa)}_{j_\kappa} \mid h^{(\kappa)} \mid \varphi^{(\kappa)}_{l_\kappa} \rangle A_{l_1 \dots l_f} \\ &+ \sum_{r=1}^{s} c_r \Bigg(\sum_{l_1} \langle \varphi^{(1)}_{j_1} \mid h^{(1)}_r \mid \varphi^{(1)}_{l_1} \rangle \dots \\ &\times \Bigg(\sum_{l_f} \langle \varphi^{(f)}_{j_f} \mid h^{(f)}_r \mid \varphi^{(f)}_{l_f} \rangle A_{l_1 \dots l_f} \Bigg) \Bigg) \\ = &\sum_{L} \boldsymbol{\mathcal{K}}_{JL} A_L ,\end{aligned} \tag{27}$$

where we have implicitly defined the *A-Hamiltonian matrix* $\boldsymbol{\mathcal{K}}$. (Contrary to (26), here "…" does contain l_κ.) Recognize that $\boldsymbol{\mathcal{K}}$ depends on the single-particle functions which in turn depend on the MCTDH-coefficients, making (27) non-linear.

To arrive at equations that can be implemented, the single-particle functions have to be represented by a finite set of numbers. This can be achieved by employing a collocation scheme of the fast Fourier transform (FFT) [3,5] or the discrete variable representation (DVR) [4,6,43,44] type. In these schemes the single-particle function $\varphi^{(\kappa)}_j$ is represented by its values on a set of N_κ grid points or, equivalently, is expanded in a set of N_κ *primitive* basis functions. In the following we will assume for simplicity that the single-particle functions are represented on a DVR grid.

C Computational effort

In order to construct an efficient integration scheme tailored to the MCTDH equations of motion it is instructive to investigate the computational effort required to evaluate the right hand side of the MCTDH working equations (13) and (14). We define the effort as the number of floating point operations to be carried out and consider only the most important terms. For the sake of simplicity we assume that the number of grid points or primitive basis functions, N, as well as the number of single-particle functions, n, does not depend on the particular degree of freedom κ. Alternatively, one may consider N and n as the geometric means of the N_κ and n_κ, respectively. Notice that in the MCTDH applications N is typically much larger than n. We also presume for the moment that the single-set formulation is applied. Since the computational effort has been determined in detail in a previous work [17] we only summarize the results.

The effort of the MCTDH algorithm can be split up into two parts with different scaling behavior. For small values of n and f, that is for systems with comparatively little correlation and few degrees of freedom, the dominant contribution to the computational effort stems from the calculation of the action of the single-particle operators $h^{(\kappa)}_r$ on the single-particle functions $|\varphi^{(\kappa)}_j\rangle$. This effort grows linearly with the number of degrees of freedom and is proportional to $sfnN^2$.

For systems where n and f are large, the calculation of the derivative of the MCTDH-coefficients and in particular the mean-field matrices determines the numerical cost, which scales exponentially with the number of modes f. The effort for computing the mean-field matrices is proportional to sf^2n^{f+1}. The cost to determine the time-derivative (27) of the MCTDH-coefficients scales with sfn^{f+1}. Note,

however, that the right hand side of (27) is evaluated in almost the same way as the mean-field matrix elements $\boldsymbol{\mathcal{H}}^{(\kappa)}_{rjl}$, (26), which allows the computation of i$\dot{\mathbf{A}}$ as a by-product of the calculation of the mean-field matrices with only little additional cost.

For comparision, in the standard method of representing the wave function on a time-independent product DVR grid the effort is proportional to fN^{f+1}. For systems with large values of n and f the gain factor of the MCTDH scheme with respect to the standard method is hence proportional to $s^{-1}f^{-1}\,(N/n)^{f+1}$. Consequently, the MCTDH scheme is superior over the standard method if the number of degrees of freedom as well as the *contraction efficiencies* N_κ/n_κ, and in particular the mean contraction efficiency N/n, are sufficiently large.

So far we have restricted our discussion to the single-set formulation. The single-set formulation has the advantage over the multi-set approach that only one set of single-particle functions (instead of σ) must be propagated. On the other hand, since in the multi-set formulation a separate set of functions is used for each electronic state, the number of single-particle functions per state that is required for convergence is typically smaller than in the single-set formulation. This is because each set of single-particle functions individually adapts itself to the wave-packet of the corresponding state. Note that the number of single-particle functions per state contributes to the exponentially growing effort of the MCTDH algorithm, while the number of sets only affects the linearly scaling parts. This favors the multi-set approach in many cases. In Sect. IV we present calculations employing both the single- and the multi-set formulation.

III An integration scheme tailored to MCTDH

A The basic ideas

Having discussed the MCTDH equations of motion and the computational effort of solving them, we shall now develop an integration scheme that is both more efficient and robust in handling the MCTDH working equations.

Let us first recapitulate the main bottlenecks of the MCTDH algorithm in order to find the shortcomings an efficient integration scheme can attack:

1. The wave function, i. e. the A-vector and the single-particle functions, contains parts that are highly oscillatory in time. This eventually enforces small integration steps.
2. During the propagation the density and mean-field matrices have to be computed at each integration step. Remember that the effort for these calculations grows exponentially with the number of degrees of freedom.
3. The set of ordinary differential equations (13) and (14) is non-linear, inhibiting the use of such powerful integrators as the Chebyshev [1] or the short iterative Lanczos [45] scheme.
4. The (residual part of the) Hamiltonian must be expanded in a product representation (23). The computational cost of the integration grows linearly with the number of these expansion terms.

Two comments on this list should be made. Firstly, in some cases the problem of small integration steps can be somewhat reduced by moving from the Schrödinger picture to an interaction picture for the propagation of the single-particle functions [32]. In the interaction picture the time-derivative of the single-particle functions is formed employing the residual Hamiltonian only, which might cause the single-particle functions to change less rapidly. For the pyrazine molecule [32], for instance, integration steps about twice as large were possible in the interaction picture. This indicates that the fast oscillating terms in the wave function belong to the single-particle functions rather than the MCTDH-coefficients.

The second comment refers to the difficulties that arise for large expansions of the residual Hamiltonian, as mentioned in the last item. An alternative to this expansion (23) is the so-called correlated DVR (CDVR) that has recently been suggested by Manthe [46]. The concept behind this method is to use the single-particle functions in order to create a small time-dependent DVR grid and to evaluate the potential on these DVR points. This avoids the need of expanding the residual Hamiltonian in a product representation. Since the CDVR method is at present still in a stage of development we will assume in the following that the Hamiltonian is given in the product form (23). We want however to emphasize that the integration scheme to be described below can be made compatible with the CDVR method, at the cost of additional storage.

The main idea underlying our integration scheme is motivated by the realization that the matrix elements $\boldsymbol{\mathcal{K}}_{JL} = \langle \Phi_J \,|\, H \,|\, \Phi_L \rangle$ and the product of the inverse density and the mean-field matrices, $\left(\boldsymbol{\rho}^{(\kappa)}\right)^{-1} \boldsymbol{\mathcal{H}}^{(\kappa)}_r$, generally change much slower than the MCTDH-coefficients and the single-particle functions. For that reason it might be possible to use a wider meshed time discretization for the propagation of the former quantities than for the latter ones with only a minor loss of accuracy. In other words, during the integration of the equations of motion (13) and (14) one may hold the matrix elements, the density matrices, and the mean-field matrices constant for some time τ.

This concept shall now be discussed in more detail. For the sake of simplicity we first consider a simplified variant that already demonstrates most of the properties and advantages of the integrator. The actual integration scheme is somewhat more subtle and is described in the subsequent Sect. III.B. An integration step in this simplified variant begins with the initial values $\mathbf{A}(t_0)$ and $\boldsymbol{\varphi}^{(\kappa)}(t_0)$ being employed to determine the A-Hamiltonian matrix $\boldsymbol{\mathcal{K}}(t_0)$ (27), the regularized density matrices $\boldsymbol{\rho}^{(\kappa)}(t_0)$ (10) and (22), and the mean-field matrices $\boldsymbol{\mathcal{H}}^{(\kappa)}_r(t_0)$ (26). With these matrices kept constant, the wave function is then propagated from t_0 to $t_1 = t_0 + \tau$. The propagated values $\mathbf{A}(t_1)$ and $\boldsymbol{\varphi}^{(\kappa)}(t_1)$ are used to compute $\boldsymbol{\mathcal{K}}(t_1)$, $\boldsymbol{\rho}^{(\kappa)}(t_1)$, and $\boldsymbol{\mathcal{H}}^{(\kappa)}_r(t_1)$. This procedure is reiterated until the desired final point of time is reached.

In the single-set formulation the *discretized MCTDH equations of motion* then read

$$\mathrm{i}\dot{A}_J(t) = \sum_L \bar{\boldsymbol{\mathcal{K}}}_{JL} A_L(t) \tag{28}$$

$$
\begin{aligned}
\mathrm{i}\dot{\varphi}_j^{(1)}(t) = \left(1 - P^{(1)}\right) \Bigg(& h^{(1)}\varphi_j^{(1)}(t) + \sum_{k,l=1}^{n_1} \left(\bar{\rho}^{(1)\,-1}\right)_{jk} \\
& \times \sum_{r=1}^{s} \bar{\mathcal{H}}_{rkl}^{(1)} h_r^{(1)} \varphi_l^{(1)}(t) \Bigg) \\
\vdots \qquad & \qquad\qquad \vdots \qquad\qquad (29) \\
\mathrm{i}\dot{\varphi}_j^{(f)}(t) = \left(1 - P^{(f)}\right) \Bigg(& h^{(f)}\varphi_j^{(f)}(t) + \sum_{k,l=1}^{n_f} \left(\bar{\rho}^{(f)\,-1}\right)_{jk} \\
& \times \sum_{r=1}^{s} \bar{\mathcal{H}}_{rkl}^{(f)} h_r^{(f)} \varphi_l^{(f)}(t) \Bigg) .
\end{aligned}
$$

The bar indicates that the corresponding term is evaluated at the time $t_i = t_0 + i\tau$, with i being the number of steps made so far, and is then held constant over the integration step $t_i \le t \le t_{i+1}$. Analogous equations hold for the multi-set formulation.

Supposing the step size τ can be chosen comparatively large, the new integration scheme has several advantages. First of all, the density and mean-field matrices have to be set up less frequently. Since for large systems – i. e. for systems with many configurations (6) and a long expansion of the Hamiltonian (23) – the calculation of the mean-field matrices dominates the numerical effort, our integration scheme significantly reduces the computation time. The overhead created by the product form (23) of the Hamiltonian is diminished, too.

Another important characteristic of the new integration scheme lies in the simplified structure of the system of differential equations. While the MCTDH equations (13) and (14) are coupled, the discretized equations (28) and (29) separate into $f + 1$ disjoined subsystems. One of these subsystems is for the MCTDH-coefficients, the others are for each of the f single-particle vectors $\boldsymbol{\varphi}^{(\kappa)}$ (11). Splitting a large system of differential equations into smaller ones generally lessens the computational effort because the step size can then be adapted independently for each subsystem; if one subsystem requires small integration steps, the others remain unaffected. Furthermore, the decoupling of the working equations allows the integration of each subsystem with a different accuracy. For example, since for molecules with many degrees of freedom the effort for the propagation of the single-particle functions can be neglected, one might integrate the set of equations (29) with high precision, while demanding only a moderate accuracy for the expensive integration of (28).

Finally, we point out that the working equation (28) for the A-vector is linear with constant coefficients, which permits the solution by integrators explicitly designed for equations of that kind [2], such as the Chebyshev [1] or Lanczos [45] method. For a large system the cost for the integration of the equations of motion (28) and (29) is almost entirely caused by the propagation of the A-vector since its length by far exceeds the length of the single-particle vectors. This underlines the importance of applying an efficient integrator to the propagation of the MCTDH-coefficients. The set of equations (29), however, is still non-linear because of the projection operator $P^{(\kappa)}$.

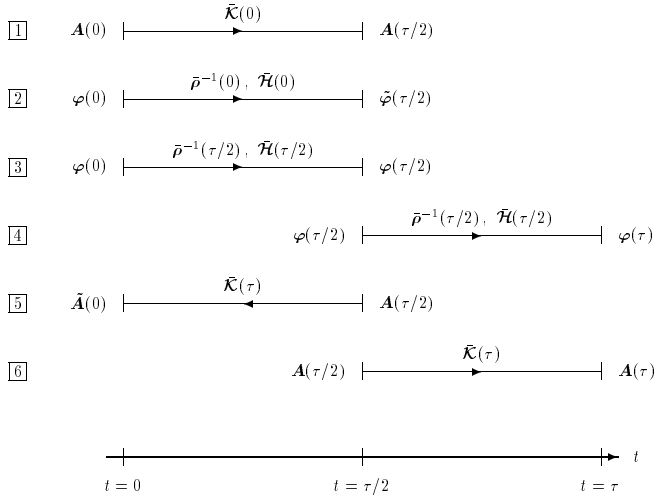

Fig. 1. Diagrammatic description of the integration scheme. See text for details

As a résumé one can say that our integration scheme has a good chance of at least diminishing and partly even removing the bottlenecks of the MCTDH algorithm mentioned at the very beginning of this section.

B The integration scheme

Despite all its advantages, the simple integration scheme depicted in the previous Sect. III.A has to be improved further for two reasons in order to be competetive. The first one is that in its current form the method defines – analogous to Euler's rule – a first order integrator, which are known to perform quite poorly. The second reason is that our scheme lacks a means of estimating the discretization error and adjusting the step size τ. The following modifications of the method eliminate these shortcomings.

The modified integration scheme is depicted in Fig. 1. This diagram displays a step of size τ from time $t = 0$ to $t = \tau$. $\bar{\mathcal{K}}(t)$, $\bar{\rho}^{-1}(t)$, and $\bar{\mathcal{H}}(t)$ denote the A-Hamiltonian, the inverse density and the mean-field matrices, respectively, evaluated at the time t and held constant during the integration step (we have dropped the superscript κ for simplicity). First, the wave function at time $t = 0$ is used to determine $\bar{\mathcal{K}}(0)$, $\bar{\rho}^{-1}(0)$, and $\bar{\mathcal{H}}(0)$. Then both the MCTDH-coefficients (step 1 in the figure) and the single-particle functions (step 2) are propagated from $t = 0$ to $t = \tau/2$ according to (28) and (29), yielding $\mathbf{A}(\tau/2)$ and $\tilde{\boldsymbol{\varphi}}(\tau/2)$. With this propagated wave function the advanced $\bar{\rho}^{-1}(\tau/2)$, and $\bar{\mathcal{H}}(\tau/2)$ are computed and employed in a second propagation of the single-particle functions from $t = 0$ to $t = \tau/2$ (step 3), resulting in $\boldsymbol{\varphi}(\tau/2)$. The difference between $\boldsymbol{\varphi}(\tau/2)$ and $\tilde{\boldsymbol{\varphi}}(\tau/2)$ measures the error of the single-particle functions caused by the discretization. We will soon address this error in detail, but for the moment it is sufficient to know that if this error is too large the integration step made so far is rejected and repeated with a smaller step size τ, otherwise the step is accepted and $\boldsymbol{\varphi}$ is propagated to the end of the interval, $t = \tau$, (step 4). The knowledge of $\boldsymbol{\varphi}(\tau)$ allows the calculation of the A-Hamiltonian matrix $\bar{\mathcal{K}}(\tau)$. To obtain an error estimate for the MCTDH-coefficients, $\mathbf{A}(\tau/2)$ is then propagated back-

wards in time from $t = \tau/2$ to $t = 0$ employing $\bar{\boldsymbol{\mathcal{K}}}(\tau)$ (step 5), leading to $\tilde{\mathbf{A}}(0)$. Again, the difference between the initial $\mathbf{A}(0)$ and $\tilde{\mathbf{A}}(0)$ is linked to the error of the coefficients due to the discretization and is used to decide whether to reject or accept the integration step. In the latter case, $\mathbf{A}(\tau/2)$ is propagated over the second half of the interval (step 6), yielding $\mathbf{A}(\tau)$. The step is completed by the calculation of $\bar{\boldsymbol{\rho}}^{-1}(\tau)$ and $\bar{\boldsymbol{\mathcal{H}}}(\tau)$.

In the following we will call this integration scheme the *constant mean-field* (CMF) integrator. Remember, however, that not only the mean-fields but also the A-Hamiltonian and the density matrices are held constant. When, on the other hand, the original MCTDH-equations (13) and (14) are solved (without keeping any mean-fields fixed) we will speak of the *variable mean-field* (VMF) method.

We will now detail how the error estimate and the step size control are implemented in the CMF scheme. To this end we have to know how the differences $\Delta\mathbf{A} = \tilde{\mathbf{A}} - \mathbf{A}$ and $\Delta\boldsymbol{\varphi}^{(\kappa)} = \tilde{\boldsymbol{\varphi}}^{(\kappa)} - \boldsymbol{\varphi}^{(\kappa)}$ are connected to the error of the wave function. Let Ψ and $\tilde{\Psi}$ denote two MCTDH wave functions (1). Expanding the difference between Ψ and $\tilde{\Psi}$, one obtains in lowest order

$$\| \Psi - \tilde{\Psi} \|^2 = \| \Delta\mathbf{A} \|^2 + \sum_{\kappa=1}^{f} \mathrm{tr}\left(\Delta\boldsymbol{\mathcal{O}}^{(\kappa)} \boldsymbol{\rho}^{(\kappa)\,T} \right) , \tag{30}$$

with $\Delta\mathcal{O}^{(\kappa)}_{jl} = \langle \Delta\varphi^{(\kappa)}_j \mid \Delta\varphi^{(\kappa)}_l \rangle$. Setting $\Delta\boldsymbol{\varphi} = \tilde{\boldsymbol{\varphi}}(\tau/2) - \boldsymbol{\varphi}(\tau/2)$ and $\Delta\mathbf{A} = \tilde{\mathbf{A}}(0) - \mathbf{A}(0)$, we thus define the (absolute) CMF discretization error of the MCTDH-coefficients and the single-particle functions as

$$\delta_A = \frac{1}{4} \| \Delta\mathbf{A} \|^2 \tag{31}$$

and

$$\delta_\varphi = \sum_{\kappa=1}^{f} \mathrm{tr}\left(\Delta\boldsymbol{\mathcal{O}}^{(\kappa)} \boldsymbol{\rho}^{(\kappa)\,T} \right) , \tag{32}$$

respectively. (The origin of the factor $1/4$ in the definition of δ_A is explained below.) If complex absorbing potentials are employed in the calculation, the absolute errors (31) and (32) have to be replaced by relative ones. However, it seems reasonable – and our experience confirms this – that the accuracy which is necessary to compute observable quantities decreases if the norm of the wave function has almost vanished. For that reason, we redefine the errors δ_A and δ_φ as

$$\delta_A = \frac{1}{4} \frac{5 \| \Delta\mathbf{A} \|^2}{4 \| \mathbf{A} \|^2 + \| \mathbf{A} \|} \tag{33}$$

and

$$\delta_\varphi = \sum_{\kappa=1}^{f} \frac{5\,\mathrm{tr}\left(\Delta\boldsymbol{\mathcal{O}}^{(\kappa)} \boldsymbol{\rho}^{(\kappa)\,T} \right)}{4\,\mathrm{tr}\left(\boldsymbol{\rho}^{(\kappa)} \right) + \sqrt{\mathrm{tr}\left(\boldsymbol{\rho}^{(\kappa)} \right)}} . \tag{34}$$

This artificially reduces the relative error and hence enlarges the step size when the norm of the wave function tends towards zero. The numbers 4 and 5 have been found empirically to be a good choice.

A step size control not only requires a measure of the error; one also has to know how this error is linked to the step size τ. To simplify the notation we rewrite the discretized equations of motion (28) and (29) as

$$\dot{\mathbf{A}}(t) = f\left(\vartheta, \mathbf{A}(t)\right) \quad \text{and} \quad \dot{\boldsymbol{\varphi}}(t) = g\left(\vartheta, \boldsymbol{\varphi}(t)\right) . \tag{35}$$

The parameter ϑ specifies at what time $\bar{\boldsymbol{\mathcal{K}}}(\vartheta)$, $\bar{\boldsymbol{\rho}}^{-1}(\vartheta)$, and $\bar{\boldsymbol{\mathcal{H}}}(\vartheta)$ are evaluated. Equation (35) leads to the relations

$$\Delta\mathbf{A} = \int_0^{\tau/2} f(0, \mathbf{A}(t'))\, dt' + \int_{\tau/2}^{0} f(\tau, \mathbf{A}(t'))\, dt' , \tag{36}$$

$$\Delta\boldsymbol{\varphi} = \int_0^{\tau/2} g(0, \boldsymbol{\varphi}(t'))\, dt' - \int_0^{\tau/2} g(\tau/2, \boldsymbol{\varphi}(t'))\, dt' . \tag{37}$$

Expanding f and g as Taylor series in ϑ, $f(\vartheta, \cdot) = f(0, \cdot) + \vartheta f_\vartheta(0, \cdot) + O(\vartheta^2)$ (and analogously for g), one obtains

$$\| \Delta\mathbf{A} \| = \frac{\tau^2}{2} \| f_\vartheta(0, \mathbf{A}(\xi)) \| + O(\tau^3) , \tag{38}$$

$$\| \Delta\boldsymbol{\varphi} \| = \frac{\tau^2}{4} \| g_\vartheta(0, \boldsymbol{\varphi}(\xi')) \| + O(\tau^3) , \tag{39}$$

with $\xi, \xi' \in [0, \tau/2]$. The index ϑ denotes the partial derivative with respect to the first argument. Equations (38) and (39) induce the sought proportionalities $\delta_A \sim \tau^4$ and $\delta_\varphi \sim \tau^4$. Furthermore, the reason for the factor $1/4$ in the definition (31) of δ_A now becomes clear. For the backward propagation of $\mathbf{A}$ from $t = \tau/2$ to $t = 0$ (step 5 in Fig. 1) we namely use $\bar{\boldsymbol{\mathcal{K}}}(t = \tau)$, whereas in the case of the single-particle functions $\bar{\boldsymbol{\rho}}^{-1}(t = \tau/2)$ and $\bar{\boldsymbol{\mathcal{H}}}(t = \tau/2)$ are employed in computing δ_φ. Due to this factor of two in the operator's time interval the error estimates of the MCTDH-coefficients and the single-particle functions are treated unequally, as can be seen from the different prefactors in (38) and (39). The factor $1/4$ has been introduced in definition (31) to remove this inconsistency.

Having found the scaling behavior $\delta_A \sim \tau^4$ and $\delta_\varphi \sim \tau^4$, it is now possible to adjust the size of the steps by comparing the error $\delta = \max(\delta_A, \delta_\varphi)$ to an error tolerance ϵ that defines the accuracy of the calculation. If $\delta > 2\epsilon$ we reject and repeat the step, otherwise we accept it. In both cases we set the new step size τ_{new} to

$$\tau_{\mathrm{new}} = \tau \sqrt[4]{\epsilon/\delta} , \tag{40}$$

with τ being the current step size. For a repetition step, τ_{new} is further reduced by a safety factor of 0.8. If a step is accepted, we impose the constraint $\tau_{\mathrm{new}} \leq 1.5\tau$ on the new step size in order to hinder the steps from being enlarged too rapidly. Moreover, we modify the step size such that the time interval until the next output of data becomes an integer multiple of τ_{new}. Otherwise a very small step size might be necessary at the end of the remaining interval to hit exactly the point of time of the next output.

Because $\|\tilde{\mathbf{A}}(0) - \mathbf{A}(0)\|$ and $\|\tilde{\boldsymbol{\varphi}}(\tau/2) - \boldsymbol{\varphi}(\tau/2)\|$ are computed with the MCTDH-coefficients and the single-particle functions being propagated using different $\bar{\boldsymbol{\mathcal{K}}}$, $\bar{\boldsymbol{\rho}}^{-1}$, and $\bar{\boldsymbol{\mathcal{H}}}$, they are sensitive to the changes of the A-Hamiltonian, the density and the mean-field matrices, respectively. These errors are thus proportional to τ^2. Notice, however, that the single-particle functions are propagated using $\bar{\boldsymbol{\rho}}^{-1}$ and $\bar{\boldsymbol{\mathcal{H}}}$ evaluated at the midpoint $t = \tau/2$ of a CMF step. For the

propagation of the A-vector, $\bar{\boldsymbol{\mathcal{K}}}(0)$ is employed in the first and $\bar{\boldsymbol{\mathcal{K}}}(\tau)$ in the second half-step. Hence we realize that the CMF scheme defines a midpoint method in the case of the single-particle functions and a trapezoidal rule for the MCTDH-coefficients [47]. The order of the local discretization error, i. e. the additional error of the wave function introduced by a single CMF step, is therefore higher by one than the error of the mean-fields, namely proportional to τ^3. Since for any one-step method the order of the global discretization error, defined as the error over a fixed propagation time, is a power one lower than that of the local error [47], we recognize that our scheme actually controls the global rather than the local error. We also identify the CMF integrator as a second order method.

We still need to comment on how (28) and (29) are being integrated. For the propagation of the MCTDH-coefficients we take advantage of the linearity of (28) as well as the hermiticity of the A-Hamiltonian matrix $\bar{\boldsymbol{\mathcal{K}}}$ and employ a short iterative Lanczos (SIL) [45] integrator with variable order. (If complex absorbing potentials are included in the Hamiltonian, then $\bar{\boldsymbol{\mathcal{K}}}$ is no longer hermitian. In such a case the SIL-integrator is replaced by a Lanczos-Arnoldi integrator [48–50].) The Lanczos scheme possesses several properties that make the CMF integrator not only efficient but also robust and easy to handle. For instance in the SIL method, no knowledge of the energy range, and no energy shift of the Hamiltonian is required; it is also less sensitive to large eigenvalues of the Hamiltonian than other polynomial methods. Moreover, the Lanczos algorithm conserves the norm exactly, whereas in a VMF calculation the norm is generally not strictly conserved due to numerical inaccuracies. The CMF integrator profits from a further feature of the Lanczos scheme. In order to estimate the integration error of the MCTDH-coefficients, the CMF method demands a backward propagation of the A-vector (step 5 in Fig. 1). The SIL-integrator now permits the estimation of this error almost for free, as the Krylov space that has to be built for this back-propagation can also be used in the subsequent forward propagation (step 6).

Since (29) is non-linear, the Lanczos method cannot be applied to the single-particle functions. In the VMF approach, of all the integrators we have tested an Adams-Bashforth-Moulton (ABM) predictor-corrector turned out to perform most efficiently in integrating the complete set (13) and (14) of differential equations. However, a multistep method like ABM is not very appropriate to the CMF scheme because it has to be restarted twice within each CMF step. To integrate (29) we therefore employ a Bulirsch-Stoer (BS) extrapolation method with variable order, variable step size, and polynomial extrapolation [51].

In the previous section III.A we have already underlined the various benefits of the simplified version of our integration scheme. The CMF method offers two important additional advantages. First of all, the CMF integrator enables one to control the discretization error and adjust the step size. Without such an internal error control it would hardly be possible to apply the integrator to realistic problems where nothing or only little is known about the exact solution, and hence no comparision between the obtained and the exact results can be made. The second and also very important improvement lies in increasing the order of the error term and thus allowing larger CMF step sizes.

The major disadvantage of the CMF strategy compared to the simplified scheme discussed in Sect. III.A is the one and a half fold increase in the effort of propagating the single-particle functions. For large systems however (i. e. for $n^f \gg N^2$) most of the computation time is spent on the propagation of the MCTDH-coefficients, so that this additional cost is negligible.

We close this section in emphasizing that the CMF integration scheme converges for $n \to N$ towards the standard method of representing the wave function in a time-independent product basis set: for $n = N$ both the single-particle functions and the mean-fields are constant. Moreover, the CMF integrator conserves the norm exactly. Unlike the VMF scheme, however, the energy is not strictly conserved. Finally, we point out that due to the independent propagation of the MCTDH-coefficients and the single-particle functions, the CMF integrator is well suited for parallelization, for example on a workstation cluster.

C Computational details

For an efficient implementation of the CMF integrator described in Sect. III.B one should pay attention to some technical details.

The first one concerns the propagation of the single-particle functions according to (29). As pointed out in Sect. II.C this dominates the numerical cost for small systems. Although the mean-field matrices $\bar{\boldsymbol{\mathcal{H}}}^{(\kappa)}_r$ are constant, the sum

$$\sum_{r=1}^{s} \bar{\boldsymbol{\mathcal{H}}}^{(\kappa)}_{rkl}\, h^{(\kappa)}_r \varphi^{(\kappa)}_l \tag{41}$$

still has to be computed at each evaluation of the right hand side of (29). To explore how one can circumvent this summation we examine the value of the vector (41) at the αth ($\alpha = 1, \ldots, N_\kappa$) grid point. Let $|\, q^{(\kappa)}_\alpha\rangle$ denote the corresponding DVR-function. Projecting (41) onto $|\, q^{(\kappa)}_\alpha\rangle$ and utilizing the fact that the set of DVR-functions is (numerically) complete we obtain

$$\begin{aligned} &\langle q^{(\kappa)}_\alpha \mid \sum_{r=1}^{s} \bar{\boldsymbol{\mathcal{H}}}^{(\kappa)}_{rkl}\, h^{(\kappa)}_r \mid \varphi^{(\kappa)}_l \rangle \\ &\quad = \sum_{\beta=1}^{N_\kappa} \left(\sum_{r=1}^{s} \bar{\boldsymbol{\mathcal{H}}}^{(\kappa)}_{rkl}\, \langle q^{(\kappa)}_\alpha \mid h^{(\kappa)}_r \mid q^{(\kappa)}_\beta \rangle \right) \langle q^{(\kappa)}_\beta \mid \varphi^{(\kappa)}_l \rangle \,. \end{aligned} \tag{42}$$

The number in brackets could in principal be determined for all κ, α, β, k and l only once at the beginning of each CMF step and then taken from memory. However, this would require the storage of fn^2N^2 complex numbers. Since most of the single-particle operators are potential terms and hence diagonal, it seems reasonable to save only these terms and continue treating the non-diagonal ones as before. For simplicity let us assume that the Hamiltonian expansion terms are arranged such that the first s_κ are diagonal, i. e. $\langle q^{(\kappa)}_\alpha \mid h^{(\kappa)}_r \mid q^{(\kappa)}_\beta \rangle = \langle q^{(\kappa)}_\alpha \mid h^{(\kappa)}_r \mid q^{(\kappa)}_\alpha \rangle\, \delta_{\alpha\beta}$, whereas the other $s - s_\kappa$ are represented by full matrices. Expression (42) then reads

$$\langle q_\alpha^{(\kappa)} \mid \sum_{r=1}^{s} \bar{\mathcal{H}}_{rkl}^{(\kappa)}\, h_r^{(\kappa)} \mid \varphi_l^{(\kappa)} \rangle = \mathcal{M}_{kl\alpha}^{(\kappa)}\, \langle q_\alpha^{(\kappa)} \mid \varphi_l^{(\kappa)} \rangle + \sum_{r=s_\kappa+1}^{s} \bar{\mathcal{H}}_{rkl}^{(\kappa)}\, \langle q_\alpha^{(\kappa)} \mid h_r^{(\kappa)} \mid \varphi_l^{(\kappa)} \rangle\,, \tag{43}$$

with

$$\mathcal{M}_{kl\alpha}^{(\kappa)} = \sum_{r=1}^{s_\kappa} \bar{\mathcal{H}}_{rkl}^{(\kappa)}\, \langle q_\alpha^{(\kappa)} \mid h_r^{(\kappa)} \mid q_\alpha^{(\kappa)} \rangle\,. \tag{44}$$

Since $\bar{\mathcal{H}}$ is constant, $\mathcal{M}$ needs to be computed only initially at each CMF (half-) step. The numerical effort of calculating the diagonal part of sum (42) is then reduced by a factor of s_κ for each degree of freedom κ, diminishing the handicap of the restricted form of the residual Hamiltonian (23).

The second item refers to the adaptation of the step size. When the CMF integrator is applied to realistic problems, where the interest lies in calculating observable quantities, one usually needs the solution Ψ of the equations of motion at certain (typically equidistant) times t_i. According to Heisenberg's uncertainty principle, the distance Δt between two neighboring points t_i and t_{i+1} must be chosen sufficiently small in order to resolve the full energy range. Since the step size τ is limited by $\tau \leq \Delta t$ this might affect the length of the CMF steps and hence reduce the integrator's efficiency. In those cases where the observables (e. g. spectra) are determined using the autocorrelation function a simple trick exists that enables one to double the output interval Δt. The autocorrelation function at $t = t_i$ is defined as $c(t_i) = \langle \Psi(0) \mid \Psi(t_i) \rangle$. If the initial value $\Psi(0)$ is real, the autocorrelation function can be written $c(2t_i) = \langle \Psi^*(t_i) \mid \Psi(t_i) \rangle$ [52, 53]. Because this notation allows the propagation of the wave function Ψ over only half the time for which the autocorrelation function is required, this is the preferable way to compute $c(t)$. However, the autocorrelation function is then given solely at the times $2i\Delta t$ instead of $i\Delta t$ ($i = 0, 1, \ldots$). At the missing intermediate points $(2i-1)\Delta t$ the autocorrelation function can be obtained by $c((2i-1)\Delta t) = \langle \Psi^*((i-1)\Delta t) \mid \Psi(i\Delta t) \rangle$, provided that $\Psi((i-1)\Delta t)$ has been saved in memory. This permits the choice of a Δt twice as large as before at the price of one extra Ψ-vector that must be stored.

Having described the CMF integration scheme in detail, we shall now estimate what speed-up of a CMF calculation compared to a VMF calculation one can expect. We restrict our discussion to large systems (i. e. $n^f \gg N^2$) where the dominant contribution to the numerical effort is caused by the computation of the mean-field matrices and the time-derivative of the MCTDH-coefficients. In the VMF scheme we usually solve the equations of motion employing an ABM predictor-corrector routine that evaluates the differential equation twice in each step. As outlined in Sect. II.C this requires $2c_1 s f^2 n^{f+1}$ floating point operations per ABM step, where c_1 is a proportionality constant. In a CMF calculation with a Lanczos integrator of (mean) order $\bar{l}$ used for the propagation of the A-coefficients $2c_1 s f^2 n^{f+1} + 2c_2 \bar{l} s f n^{f+1}$ floating point operations are needed for the two CMF half-steps. In our implementation of the code the constants c_1 and c_2 fulfil the relation $c_2 \approx 2c_1$. The gain of a CMF calculation with respect to a VMF calculation is hence approximately given by

$$\text{gain(CMF/VMF)} \approx \frac{f}{f + 2\bar{l}}\, \frac{\bar{\tau}_{\text{CMF}}}{\bar{\tau}_{\text{VMF}}}\,, \tag{45}$$

with $\bar{\tau}_{\text{CMF}}$ and $\bar{\tau}_{\text{VMF}}$ being the average CMF and VMF (i. e. ABM) step size, respectively. In the limit $f \to \infty$ the gain is exclusively given by the ratio of the CMF and the VMF step size.

We also want to estimate the gain of the CMF scheme with respect to the standard method of representing the wave function in a time-independent product basis set. To this end we assume that the equations of motion of the standard method are solved employing a Lanczos integrator. The SIL step size in the standard method will then be comparable to the size of a CMF half-step, and the mean SIL order $\bar{l}$ will also be similar in both schemes. This is a rather conservative assumption since the matrix $\bar{\mathcal{K}}$ used in the CMF scheme generally has a smaller spectral range than the Hamiltonian matrix employed in the standard method. This is because $\bar{\mathcal{K}}$ is set up in the single-particle basis which is better adapted to the potential than the primitive basis used in the standard method to represent the Hamiltonian matrix. In the standard method the effort for each SIL step is given by $c_3 \bar{l} f N^{f+1}$ with $c_3 \approx c_2$. Thus one approximately obtains for the gain of a CMF calculation with respect to the standard method:

$$\text{gain(CMF/standard)} \approx \frac{2\bar{l}}{f + 2\bar{l}}\, \frac{1}{s} \left(\frac{N}{n} \right)^{f+1}\,. \tag{46}$$

We see that the CMF scheme is superior – with regard to the computational effort – over the standard method, provided that the number of modes f and the contraction efficiencies N_κ / n_κ are sufficiently large. An example system with $f = 6$, $N = 30$, $n = 5$, $s = 50$, and $\bar{l} = 10$ shall illustrate this. (These values are similar to those in the calculations described below.) For this system a calculation using the (brute force) standard method can be expected to take 4300 times longer than a CMF calculation. If the CMF run requires for this systems, say, two hours of CPU-time, the standard method would then need about one year! This shows that MCTDH makes investigations feasible that are impossible within the standard approach.

To complete our discussion on MCTDH we shall also compare the memory requirements of both MCTDH versions (VMF and CMF) and the standard method. Since for small systems the memory requirements usually do not pose a problem, we confine ourselves to large systems (i. e. $n^f \gg f N^2$, when memory is concerned) where the only important contribution to the memory comes from the A-vectors. In the VMF scheme the ABM predictor-corrector routine we usually use is driven with a fixed order p. An overall number of $(p + 6)$ A-vectors must then be held in memory (including all auxiliary vectors), yielding $(p+6)\, n^f$ complex numbers. Taking into account all A-vectors employed in the propagation, the step size control, the additional output of the autocorrelation function, as well as all auxiliary vectors, the CMF method requires the storage of $(L+6)\, n^f$ complex numbers, where L is the maximum Lanczos order needed to integrate the intervals of length $\tau/2$. Typical values for the integration order are $p = 6$ and $L = 5$ to $L = 25$. On the other hand, in the standard approach with

a Chebyshev integrator [1] taken for the propagation, four wave functions, i. e. $4N^f$ complex numbers, must be stored in memory. So the memory gain of the MCTDH scheme with respect to the standard method, defined as the ratio between the memory requirements, ranges from about $1/8\ (N/n)^f$ to $1/3\ (N/n)^f$. Typically, n is about three to ten times smaller than N, leading to impressive memory gain factors if f is comparatively large. For the above example system – assuming double precision arithmetics – the standard method would require to store 43 Gigabytes of data, which would by far exceed the memory of even the largest machines now available. On the contrary, the MCTDH algorithm with, say, L = 20 needs merely 6 Megabytes, allowing to do the same calculation on a small workstation or even a personal computer!

IV The photodissociation of CH_3I

A Definition of the system

In order to investigate the performance of the novel integration scheme in realistic problems, we have applied the CMF integrator to the photodissociation process of methyl iodide.

Since the methyl iodide molecule consists of five atoms it has fifteen independent displacements, of which six can be ascribed to the center of mass motion and the overall orientation of the molecule about its center of mass. The remaining nine degrees of freedom define the internal vibrational motion of the molecule. Following [21] and [22], we omit the deformation and asymmetric stretch of the methyl group, and use bond length and bond angle coordinates which include all five modes that retain the local C_{3v} symmetry of the methyl fragment. The chosen coordinates – which are displayed in Fig. 2 – are the C–I bond distance r_I, the H_3–C–I bending angle θ_I (the angle between the C–I axis and the axis perpendicular to the plane spanned by the three hydrogen atoms), the angle ϕ defining the direction of the bend (dihedral angle between the iodine and a methyl hydrogen), the symmetric C–H bond distance r_H, and the umbrella angle θ_H of the methyl group.

The electronic excitation that initiates the photodissociation process is modelled according to the Condon approximation as a vertical transition from the ground electronic state to the excited state, implying a constant transition dipole moment. As in [21, 22], the ground electronic state is a model potential energy surface which is constructed from an r_I- and θ_H-dependent empirical potential [55] with a harmonic bending motion at the experimental frequency and symmetric stretching motion taken from the methyl radical potential [56].

The ground state eigenfunction is determined by relaxation [57] on this ground potential energy surface. In a relaxation calculation the wave function is propagated in imaginary time and regularly renormalized to compensate for the loss of norm. When a relaxation calculation is performed within the MCTDH framework and the constraint (3) is used, it is sufficient to renormalize only the A-coefficients because the single-particle functions remain orthonormalized even for imaginary times due to the position of the projection operator in (14).

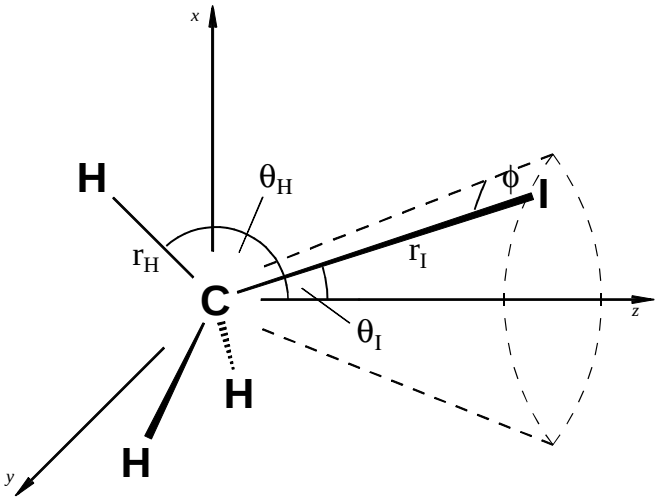

Fig. 2. The coordinate system used to describe the motion of the methyl iodide molecule in the photodissociation process

Having determined the ground state eigenfunction by such a relaxation calculation, the photodissociation process is modelled by vertically shifting this wave function to the excited $^3Q_0$ state, which correlates asymptotically with excited I* ($^2P_{1/2}$). The two $^1Q_1$ states, which correlate with ground state iodine atoms ($^2P_{3/2}$) in the dissociation limit, are also relevant for the photodissociation process and were thus included in our calculations. The diabatic potential energy surfaces and the vibronic couplings for these three excited electronic states included in our investigations are based on six-dimensional ab initio calculations [58]. The r_I, θ_I, ϕ, and θ_H dependencies of those calculations are employed in the potential surfaces and couplings of the present work. The other coordinates that were enclosed in the ab initio calculations are frozen at the C_{3v} symmetry of the methyl fragment. The symmetric C–H stretching motion is included by augmenting the methyl force field of the ab initio surfaces with an r_H- and θ_H-dependent potential for the methyl radical [22, 56].

The potential expansion terms are all included in the residual part of the Hamiltonian. Their number depends on wether one uses the single- or the multi-set formulation. In the latter formulation there are 14 potential terms for the $^3Q_0$ state, 20 for each of the two $^1Q_1$ states, and overall 18 terms that describe the vibronic couplings, yielding a total of 72 potential terms. Together with the twelve terms which make up the kinetic part of the Hamiltonian (see below) we thus have s = 108 expansion terms, since the kinetic terms act on each of the three electronic states. In the single-set formulation the number of expansion terms is smaller: there are s = 50 residual Hamiltonian terms, namely twelve kinetic and 38 potential ones.

The kinetic energy operator for the five-mode model of CH_3I can be found in [21,22]. The fourteen expansion terms given there can be rearranged in such a way that only thirteen are needed, and that all single-particle operators are hermitian [54]. By utilizing hermiticity one can almost halve the effort for determining the matrix elements $\langle\varphi_j^{(\kappa)}\,|\,h_r^{(\kappa)}\,|\,\varphi_l^{(\kappa)}\rangle$. One of the kinetic terms belongs to the separable and the remaining twelve to the residual part of the Hamiltonian.

Table 1. Representation of the single-particle functions $\varphi^{(\kappa)}$ employed in the propagation of the wave function. The numbers of single-particle functions, n_κ, is given for the single-set and – in parentheses – the multi-set calculation. The first number in parentheses refers to the $^3Q_0$ and the others to the two $^1Q_1$ states. N_κ denotes the number of grid points. "Spatial range" refers to the extension of the DVR grid. The number of single-particle functions for the multi-set calculation are chosen such that the MCTDH error is roughly the same as in the single-set calculation (see text)

Mode	Basis	n_κ	N_κ	Spatial range
r_I	FFT	6 (5,4,4)	128	3.315 a. u.–7.125 a. u.
θ_I	Legendre-DVR	5 (3,4,4)	56	0°–180°
ϕ	FFT	4 (2,3,3)	32	0°–120°
r_H	Hermite-DVR	4 (3,2,2)	16	1.5 a. u.–2.6 a. u.
θ_H	Sine-DVR	6 (6,6,6)	45	30°–150°

As mentioned in Sect. II.B the single-particle functions have to be represented on a finite set of grid points. To keep the grid length needed for the dissociative coordinate r_I small, a complex absorbing potential (CAP) [34–41] is added to the separable part of the Hamiltonian. The CAP is of the monomial form

$$V(r_I) = \begin{cases} -i\,\eta \left(r_I - r_I^{(0)}\right)^b & \text{for} \quad r_I \geq r_I^{(0)} \\ 0 & \text{for} \quad r_I < r_I^{(0)} \end{cases} . \tag{47}$$

The CAP strength η = 0.038 a. u., the order b = 3, and the initial point $r_I^{(0)}$ = 5.775 a. u. are chosen in such a way that the sum of the reflection from and the transmission through the CAP is minimized [41].

The single-particle functions are represented employing a collocation scheme of the fast Fourier transform (FFT) [3,5] or the discrete variable representation (DVR) [4, 6, 43, 44] type. The schemes and parameters we have used in our calculations are compiled in Table 1. One remark on the representation of the single-particle functions used to describe the molecule's motion in the umbrella angle θ_H should be made. The photodissociation process of methyl iodide has been studied within the MCTDH framework in [21, 22]. In these works a Legendre-DVR ranging from (nearly) $\theta_H = 0°$ to (nearly) $\theta_H = 180°$ is employed to represent the single-particle functions of the θ_H-mode. On applying the CMF scheme to this system we saw, however, that the Bulirsch-Stoer integrator was using extraordinary small steps for the integration of this particular degree of freedom. Further investigations revealed the reason for this effect: while the wave-packet obviously will never move to the unphysical regions $\theta_H \approx 0°$ or $\theta_H \approx 180°$ because of the strong repulsive forces between the hydrogen nuclei, the single-particle functions had – due to numerical inaccuracies – small contributions in these regions even soon after the beginning of the propagation. Replacing the Legendre-DVR by a Sine-DVR [59] that extends only from $\theta_H = 30°$ to $\theta_H = 150°$ eliminated this error. In a VMF calculation the same numerical problem occurs, but since the set of differential equations (13) and (14) is propagated simultaneously in this integration scheme, it would have been much more difficult to detect which degree of freedom is responsible for this. This demonstrates another virtue of the CMF method.

B Results and discussion

To investigate the most important properties of the CMF integration scheme, such as accuracy, step size, and speed-up, we shall now apply the CMF method to the photodissociation process of CH_3I. This system is described in detail in the previous Sect. IV.A.

With the first set of calculations we want to explore the dependence of the CMF scheme on the error tolerance ϵ (see (40)). To this end we propagated the wave-packet on the coupled manifold of the $^3Q_0$ and both $^1Q_1$ potential energy surfaces. The time interval was 30 fs, and the single-set formulation has been employed. No intermediate output was generated. The representations of the single-particle functions are compiled in Table 1. Remember that in the single-set formulation an extra coordinate is added to the system to represent the electronic states. For the three states included in our calculations three single-particle functions have to be used for the electronic mode. The number of configurations, i. e. the length of the A-vector, was hence 8640.

To determine the error and the gain factor of the CMF scheme we compared the CMF calculations with a VMF run where an ABM predictor-corrector of sixth order was used for the propagation of the wave function. On an 80 MHz IBM PowerPC 601 with an RS6000 processor this calculation consumed 9 h, 40 min, and 30 s of CPU-time, of which 95.2% were spent on the computation of the mean-field matrices. On the average, the ABM integrator took steps of size $\bar{\tau}_{VMF}$ = 0.0197 fs. Note that this VMF calculation required merely 3.0 MB of memory.

The CMF integrator was applied to the methyl iodide system with different error tolerances ϵ. The accuracy parameters for both the Lanczos and the BS integrator were chosen such that the errors contributed by the integrators were significantly smaller than the CMF error.

The results are compiled in Table 2. (The last three lines of the table refer to other calculations described below.) In the first column the error tolerance ϵ is given. The values range from $\epsilon = 10^{-4}$ (low accuracy) to $\epsilon = 10^{-8}$ (very high accuracy). The second column gives the accuracy of the corresponding CMF calculation. The numbers in this column are defined as

$$\begin{aligned} \text{error} &= 1 - 2\,\text{Re}\,\frac{\langle \Psi_{VMF} \mid \Psi_{CMF} \rangle}{\langle \Psi_{VMF} \mid \Psi_{VMF} \rangle + \langle \Psi_{CMF} \mid \Psi_{CMF} \rangle} \\ &= \frac{\| \Psi_{VMF} - \Psi_{CMF} \|^2}{\| \Psi_{VMF} \|^2 + \| \Psi_{CMF} \|^2} , \end{aligned} \tag{48}$$

where Ψ_{VMF} and Ψ_{CMF} stand for the wave function at the final time t = 30 fs propagated using the VMF and the CMF scheme, respectively. The denominators in (48) compensate the loss of norm due to the complex absorbing potential. The error as a function of the error tolerance is also displayed in Fig. 3. The results demonstrate that the actual error of a CMF calculation correlates closely with the selected error tolerance. This is an important property of the CMF integrator as it allows the control of the integration error very precisely. Moreover, the integration error can easily be pushed below any desired limit by choosing ϵ appropriately.

The next two columns of Table 2 denote the mean CMF step size $\bar{\tau}$ and the number of accepted CMF steps. The values in parentheses specify the number of steps that have

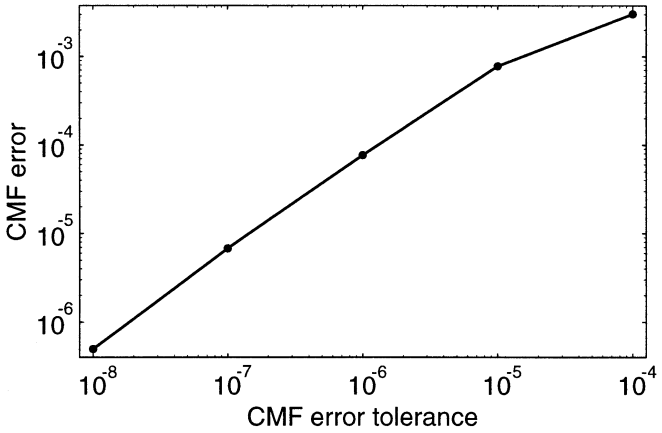

Fig. 3. The CMF error as defined in (48) versus the CMF error tolerance ϵ

been rejected and repeated with a smaller step size due to a too large error of the A-vector (first number) or the single-particle functions (second number). In the range $\epsilon = 10^{-5}$ to $\epsilon = 10^{-8}$ the mean step size falls monotonically, as one would expect since the error tolerance decreases, too. For $\epsilon = 10^{-4}$ to $\epsilon = 10^{-5}$, however, $\bar{\tau}$ shows the opposite behavior. Since these calculations have been made with comparatively low accuracy, the CMF integrator is allowed to compute a solution that can somewhat differ from the exact one. For that reason the step sizes are less predictable in this range of accuracy. The number of failed steps is relatively large for the calculations with $\epsilon = 10^{-4}$ to $\epsilon = 10^{-6}$, but in each of the two most accurate calculations with $\epsilon = 10^{-7}$ and $\epsilon = 10^{-8}$ merely two repetition steps were necessary. That the more precise calculations require less repetition steps can easily be understood because the step size control is based upon a Taylor expansion in τ and thus becomes more reliable for smaller step sizes.

Figure 4 displays the step size τ (diagram at top) and the error estimates (diagram at bottom) δ_A and δ_φ, (33) and (34), as a function of the propagation time for the calculation performed with $\epsilon = 10^{-6}$. The step size varies during the propagation by about a factor of two. This underlines the importance of adjusting τ according to the change of the A-Hamiltonian, the density and the mean-field matrices. As can be seen from the plot below, the step size is governed by both the error of the MCTDH-coefficients and the single-particle functions; in the course of the propagation there are periods where the (estimated) error of the A-vector (full line) dominates, and others where the error of the single-particle functions (dashed line) is larger.

The most interesting result of the CMF calculations is of course the gain of CPU-time with regard to a VMF calculation. The gain, which we define as the ratio between the CPU-time of the VMF and the CMF run, is also compiled in Table 2. In all calculations the gain lies well above six, and reaches a remarkable 8.6 if $\epsilon = 10^{-6}$ or $\epsilon = 10^{-7}$. Also astonishing is the dependence of the gain on ϵ. One would expect that the gain is roughly proportional to the mean step size $\bar{\tau}$. One observes, however, in the range from $\epsilon = 10^{-4}$ to $\epsilon = 10^{-6}$ the opposite behavior. Only for the more precise runs with an error tolerance between 10^{-6} and 10^{-8} does the gain satisfy the expectation.

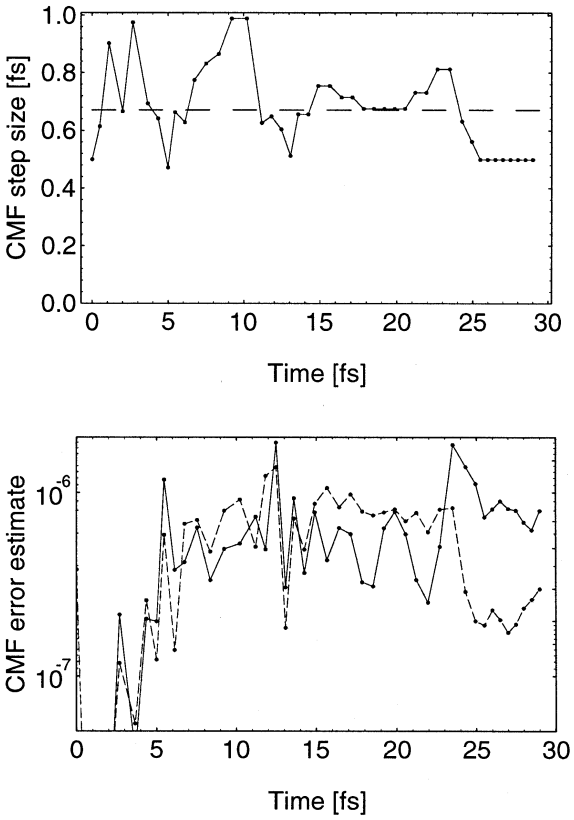

Fig. 4. Figure at *top*: The CMF step size τ as a function of the propagation time for the calculation with $\epsilon = 10^{-6}$. The *dashed line* displays the mean step size $\bar{\tau}$. Figure at *bottom*: The estimated errors δ_A (*solid line*) and δ_φ (*dashed line*) (see (33) and (34)) for the same calculation. The error estimate is shown only for those steps that have been accepted (i. e. $\max(\delta_A, \delta_\varphi) \leq 2\epsilon$)

This surprising effect is caused partly by the different numbers of repetition steps, but mainly by the Lanczos integrator. In Table 2 one finds the maximum and the mean SIL order L and $\bar{l}$, respectively. As one would presume, both the mean and the maximum Lanczos order are the larger, the larger the step size is. However, the SIL integrator is less efficient in propagating over large step sizes. In order to quantify the efficiency, we define the SIL efficiency as $c\bar{\tau}/\bar{l}$, i. e. proportional to the step size per Lanczos order, where c is chosen such that the maximum efficiency (which is reached for $\epsilon = 10^{-6}$) equals one. As indicated by the values in the table, the so defined Lanczos efficiency varies by a factor of about two, and the largest CMF gain factor is reached for the calculation with the highest SIL efficiency. We will later look closer at this effect. The efficiency of the BS integrator also varies in the different calculations, but much less dramatically than for the Lanczos method.

The next columns of Table 2 specify the absolute and – in parentheses – the relative computation time spent on the calculation of the mean-fields, the propagation of the A-vector, and the single-particle functions, respectively. The CPU-time needed to determine the mean-field matrices is larger the smaller the CMF steps are, as expected. On the other hand, the computation time for the propagation of coefficients and single-particle functions should be more or less independent of ϵ since the overall time interval to be

Table 2. Results of the CMF integration scheme for different error tolerances ϵ. The first five rows of data refer to the single-set calculations with no intermediate output, the last three lines describe the runs with the conventional Lanczos error estimate (♯), with an output interval of Δt = 0.6 fs (†) and the multi-set calculation (‡), respectively. The error in the second column is defined by (48). The next two columns denote the mean CMF step size $\bar{\tau}$ and the number of accepted CMF steps. The values in parentheses specify the number of repetition steps caused by a too large error of the A-vector (first number) or the single-particle functions (second number). The gain we define as the ratio between the CPU-time of the VMF and the CMF run. The Lanczos integrator is described by the maximum and the mean SIL order L and $\bar{l}$, respectively, as well as the SIL efficiency $c\bar{\tau}/\bar{l}$. (The constant c normalizes the most efficient calculation to one.) The next columns specify the absolute and – in parentheses – the relative computation time required for determining the mean-fields and propagating the A-vector and the single-particle functions, respectively. The VMF calculations, for comparison, require 34 830 s, 35 477 s, and 4329 s, for the Δt = 30 fs, Δt = 0.6 fs single-set and the Δt = 30 fs multi-set calculations, respectively. Finally, the last column shows the memory used in the calculations

ϵ	Error (30 fs)	$\bar{\tau}$ [fs]	Steps	Gain	L	$\bar{l}$	$c\bar{\tau}/\bar{l}$	CPU-Time[a] [s] (%) $\mathcal{H}$		$\mathbf{A}$		φ		Memory [MB]
10^{-4}	3.0×10^{-3}	0.79	38 (6,0)	6.6	21	10.5	0.62	962	(18.2)	3184	(60.1)	1002	(18.9)	4.9
10^{-5}	7.8×10^{-4}	0.86	35 (3,2)	6.5	25	12.8	0.55	862	(16.0)	3416	(63.4)	945	(17.5)	5.4
10^{-6}	7.7×10^{-5}	0.67	45 (4,1)	8.63	9	5.5	1.00	1088	(27.0)	1798	(44.5)	1038	(25.7)	3.3
10^{-7}	6.8×10^{-6}	0.51	59 (1,1)	8.57	7	4.6	0.91	1307	(32.2)	1786	(44.0)	852	(21.0)	3.1
10^{-8}	5.0×10^{-7}	0.32	93 (1,1)	6.4	6	4.1	0.64	2062	(37.9)	2503	(46.0)	715	(13.1)	2.9
10^{-4} (♯)	6.3×10^{-3}	0.81	37 (4,1)	5.0	35	16.7	0.40	919	(13.2)	4876	(70.0)	947	(13.7)	6.7
10^{-6} (†)	4.4×10^{-6}	0.60	50 (0,0)	9.9	8	5.0	0.99	1089	(30.6)	1627	(45.6)	743	(20.8)	3.2
10^{-6} (‡)	5.3×10^{-6}	0.45	66 (0,0)	1.7	5	4.0	0.92	106	(4.1)	133	(5.2)	2143	(83.8)	3.0

[a] The calculations have been performed on an 80 MHz IBM PowerPC 601 with an RS6000 processor

integrated is the same in all calculations (if one ignores the different number of repetition steps). In the case of the A-propagation, however, the effect of the variation in SIL efficiency for the different calculations is evident.

Finally, the last column of Table 2 contains the memory required by the MCTDH program. The memory mainly depends on the maximum SIL order L, since L determines the number of Lanczos vectors that have to be stored. With a maximum of 5.4 MB the memory requirements are moderate in all calculations. In the case of the three most precise calculations the memory required is similar to, or even slightly smaller than, that of the VMF run (see above).

For the six-mode methyl iodide under consideration the CMF scheme leads to a considerable reduction of the computation time. Employing (45) we shall now estimate what gain factors can be achieved for systems with a larger number f of degrees of freedom. To fix the parameters in (45) we use the VMF calculation described above and the CMF calculation performed with an error tolerance $\epsilon = 10^{-7}$, for which a speed-up of 8.3 is obtained. The latter calculation is precise enough to reproduce almost any observable in perfect agreement to a VMF calculation. The parameters are then $\bar{\tau}_{\mathrm{VMF}}$ = 0.0197 fs, $\bar{\tau}_{\mathrm{CMF}}$ = 0.508 fs and $\bar{l}$ = 4.61. Assuming that the ratio $\bar{\tau}_{\mathrm{CMF}}/\bar{\tau}_{\mathrm{VMF}}$ and the mean SIL order $\bar{l}$ are independent of f, and typical for other systems too, one can expect for a system with f = 6, 12, 24, and ∞ modes a gain factor of 10.2, 14.6, 18.6, and 25.8, respectively. The reliability of (45) can be determined by comparing the estimated gain factor of 10.2 for f = 6 with the measured result of 8.57. In this case formula (45) over-estimates the gain by about 16%. The reason for this discrepancy is that (45) has been derived for large systems neglecting in a CMF calculation the effort for the propagation of the single-particle functions, and considering in a VMF calculation exclusively the evaluation of the mean-field matrices. For the example under discussion the neglected efforts amount to 21% and 4.8% of the corresponding CPU-times, respectively. If this is taken into account, the estimated and the measured gain differ by only about one percent. Note that for large systems the share of the neglected efforts tends towards zero.

The calculations discussed above have been made without any intermediate output in order to let the CMF integrator adapt its step sizes freely. Yet usually one is interested in computing observable quantities which demands a regularly output of, for instance, the wave function or the autocorrelation function. The (maximum) output interval Δt is then dictated by the system since Δt must be small enough to resolve the full energy range. For the methyl iodide system under consideration this output interval is Δt = 0.6 fs. Therefore we have repeated both the VMF and the CMF run with $\epsilon = 10^{-6}$ using this output interval. The results are again compiled in Table 2, labelled with "†". The CMF error as a function of time is shown in Fig. 5 (solid line). Also displayed is the norm of the wave function (dashed line). One observes a comparatively slow increase of the error over the first 28 fs and a steeper increase during the last 2 fs when the wave packet runs into the CAP. Remember, however, that the error we show is a renormalized one (cf. (48)). The accuracy of this calculation can also be valued by comparing the autocorrelation function to that obtained in the VMF run. Throughout the propagation interval both the real and imaginary part of the autocorrelation function determined in the VMF and the CMF calculation differ by at most 10^{-5}. This difference in the autocorrelation function is surely small enough to be unobservable in measurable quantities, e. g. spectra. We do not discuss the photoabsorption spectrum, final state distributions etc., here, because this has been done in previous publications [21, 22].

In this particular calculation the CMF step size remains constant at 0.6 fs over the whole propagation interval. (We want to emphasize, however, that this is in general not the case. For other systems, e. g. the $H + H_2 \rightarrow H_2 + H$ exchange reaction, the step size τ is smaller than Δt and varies during the propagation.) The gain of computation time equals almost ten and is hence even larger than for each of the runs without intermediate output. Two reasons account for this somewhat surprising effect. Firstly, the run with Δt = 0.6 fs did not require repetition steps and, secondly, the SIL and the BS integrator solve the equations of motion very efficiently for a step size of 0.6 fs. This demonstrates that the

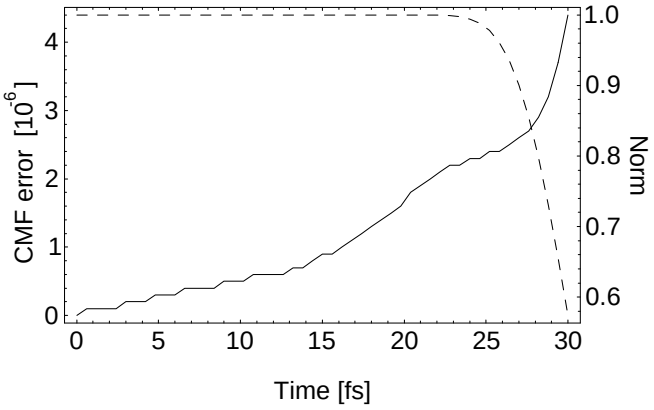

Fig. 5. The CMF error (48) as a function of the propagation time for the calculation with an output interval of 0.6 fs (*solid line*). Also given is the norm of the wave function (*dashed line*)

CMF scheme indeed yields very accurate results in much shorter CPU-time when it is applied to realistic problems.

In all our calculations formula (5) – derived in the appendix – has been employed to estimate the error of the Lanczos integrator. We emphasize that the Lanczos efficiency depends even stronger on the step size when the conventional SIL error estimate (4) is used. In order to demonstrate this we have repeated the run performed with $\epsilon = 10^{-4}$ and no intermediate output employing the conventional error estimate. The results can be found in Table 2 (labelled with "♯"). Both the maximum SIL order $L = 35$ and the mean order $\bar{l} = 16.7$ are much larger than in the corresponding calculation performed with the improved estimate (5), leading to a Lanczos efficiency of only 0.40 rather than 0.62. For large step sizes – i. e. $\bar{\beta}\bar{\tau} \gg 1$, where $\bar{\beta}$ denotes the average of the sub-diagonal elements of matrix (1) – the improved error estimate is much more reliable than the conventional one, while for small step sizes both estimates yield almost identical results.

Up to now we have concentrated on computations within the single-set formulation. For the process under consideration the multi-set formulation has the advantage that a converged result can be obtained with fewer single-particle functions per state. Because of this, the multi-set formulation is in the case of the photodissociation of CH_3I the preferable method, as it makes the system smaller with respect to the computational effort and hence reduces the CPU-time in both a VMF and a CMF calculation. In spite of this, we have decided to use the single-set formulation to investigate the CMF integrator, since the CMF scheme is especially designed to propagate large systems efficiently, so that the single-set formulation is much better suited to analyze the characteristic properties of the CMF method.

For completeness let us briefly sketch the results of the multi-set calculations given in Table 2 and labelled with "‡". In both the VMF and the CMF run, only 1692 configurations were included (rather than the 8640 in the single-set computations). For the CMF calculation we have chosen an error tolerance $\epsilon = 10^{-6}$. After the propagation the wave function has an error of 5.3×10^{-6}, so that this calculation might be compared to the single-set run with $\epsilon = 10^{-7}$, which has a similar error. The gain factor reaches only 1.7. Since the step sizes in the single- and multi-set computations are comparable, the low gain of the multi-set formulation can be attributed to the smallness of the system under investigation. (Note that the propagation of the single-particle functions requires 83.8% in the multi-set calculation.) We call a system a large one if the condition $n^f \gg N^2$ is satisfied, or more precisely, if the CMF propagation of the single-particle functions takes only a small share (less than 10%, say) of the total effort. The CH_3I model treated in the single-set formulation is thus considered as a system on the border of being large. The same model, however, becomes a small system in our nomenclature when treated in the multi-set formulation. For really large systems we expect CMF/VMF gain factors of the order of ten in both formulations.

Since the CMF algorithm introduces an additional approximation to the MCTDH scheme, it is instructive to compare the CMF error to the MCTDH error, i. e. the error of the MCTDH scheme with respect to the standard method. Because it is not feasible to perform a standard calculation for the system under discussion, we estimate the MCTDH error by comparing our VMF runs (both single- and multi-set) with calculations where we have increased each n_κ by one. (Recall that the MCTDH scheme converges towards the standard method with increasing numbers of single-particle functions.) We define the MCTDH error analogous to (48). The MCTDH error found equals 9.5×10^{-5} for the single-set calculation and 8.1×10^{-5} for the multi-set run. For a sensible error tolerance of, say, $\epsilon = 10^{-6}$ the CMF error lies thus below the MCTDH error.

Another type of calculation we have not discussed so far is the relaxation used to determine the electronic ground state eigenfunction. Such a relaxation can also be performed within the CMF method. Again we employ both the VMF and the CMF scheme (with $\epsilon = 10^{-6}$) for the relaxation and compare the results. In these single-set calculations the wave function consists of 2700 configurations. The mean CMF step size results in $\bar{\tau} = 2.1$ fs. The explanation for such a large mean step size is that during the relaxation process the wave function soon becomes nearly converged, so that the mean fields, density matrices and matrix elements change only little and can be kept constant for a rather long time. The gain factor will therefore be large, too: one obtains 6.9, which is quite a high value for a system of this size. The error of the CMF calculation lies below 10^{-7}. These results show that the CMF scheme is excellently suited not only for propagation but also for relaxation calculations.

So far we have presented calculations on the photodissociation of CH_3I. To close this section we want to mention that gain factors similar to those we have observed in these calculations can also be achieved for other systems. For example, very recently the MCTDH-algorithm has been applied to the 3-dimensional $H+H_2 \rightarrow H_2+H$ exchange reaction. In these calculations between 12 and 18 single-particle functions were used for the three degrees of freedom, yielding a total of 3456 configurations. The residual part of the Hamiltonian consisted of 254 expansion terms. Depending on the prescribed accuracy, the agreement between the results (e. g. the reaction probability) obtained in a VMF and a CMF calculation ranged from very good to perfect. The CPU-time, however, was reduced by a factor between 10 and 6, respectively, when using the CMF integrator [60].

V Summary

In the present paper, the CMF integration scheme for the working equations of the MCTDH method has been presented. By applying the CMF integrator to the photodissociation of CH_3I, we have shown that a gain in computation time over the conventional VMF integration scheme of up to ten can be reached. The loss of accuracy caused by the CMF method is on the other hand usually smaller than the original MCTDH error. We have chosen the five-dimensional CH_3I system for these tests, because we knew from previous investigations [21,22] that it is on the border of being large. A really large system would have shown even more impressive CMF/VMF gain factors but would not have allowed us to do so many test calculations.

Our investigations have also demonstrated that for the present system the multi-set formulation is much more efficient than the single-set one. To examine this system one should thus use the multi-set formulation. However, the study of the photodissociation process of CH_3I was not the aim of the present paper (we refer the interested reader to [22]); we concentrated on the single-set formulation to make our points.

The CMF integration scheme has additional advantages besides numerical efficiency over the VMF method. Since the CMF algorithm decouples the MCTDH equations of motion into $f+1$ independent subsets it is possible to choose an individual accuracy for the integration of each subset. The decoupling also allows to analyze in some detail where the numerical effort is consumed. In particular, one clearly recognizes if the solution of one set of equations takes an undue amount of time because of, for instance, an inappropriate representation. (Confer to the discussion at the end of Sect. IV.A.)

The CMF integrator also allows a quite reasonable estimation of the gain factor with respect to the standard method of using a product basis set (see (46)). Very impressive gain factors of several orders of magnitude can be achieved by the MCTDH scheme provided the mean contraction efficiency N/n is sufficiently large. From our experience we know that this contraction efficiency may become as small as two for strongly correlated systems. However, N/n typically lies in the range from three to eight and becomes in favourable cases – where the non-separable interaction is comparatively small, as for example in the photodissociation process of NOCl [17] – larger than ten. The contraction efficiency depends, of course, also on the accuracy asked for. A more approximate MCTDH calculation requires less single-particle functions, and hence shows larger contraction efficiencies.

The sometimes very large gain factors proposed by (46) must be commented on. A large system is never treated by the standard method, simply because this is not feasible. One way out is the so-called "sequential diagonalization and truncation procedure" in which adapted multi-dimensional basis sets are generated by diagonalizing model Hamiltonians of reduced dimensionality (see [61–63] and references in the latter citation). However, despite this and other impressive developments for solving the dynamics of large systems, we expect that there are many problems that can be much more efficiently solved by the MCTDH scheme than by any other method. The computation of the photoabsorption spectrum of pyrazine [32] is certainly a problem of that kind, in particular when the full dimensionality of the problem is considered [65].

The authors would like to thank A. Jäckle and G. Worth for helpful discussions and G. Worth for critically reading the manuscript. M. H. B. gratefully acknowledges financial support by the Deutsche Forschungsgemeinschaft through the Graduiertenkolleg *Modellierung und Wissenschaftliches Rechnen in Mathematik und Naturwissenschaften.*

Appendix A. The Lanczos integrator

Our calculations on the photodissociation process of methyl iodide indicate that the Lanczos scheme overestimates its integration error systematically when the step size is large. In this appendix we discuss two different error estimates for the SIL method and detail how we have estimated the SIL error in our calculations. We employ the complex Lanczos method for our considerations since it includes the hermitian Lanczos as a special case.

Let us first recall the Lanczos-Arnoldi algorithm. In the Lanczos scheme the exact Hamiltonian H is approximated by the reduced Hamiltonian $H_L = P_L H P_L$, where P_L denotes the projector on the Krylov space spanned by the set of vectors $H^k\psi(t)$, $k = 0,\ldots,L$. The Lanczos-Arnoldi recursion [48–50] is used to construct an orthonormal basis $\psi_0,\ldots,\psi_L$ in which the reduced Hamiltonian H_L is a complex upper Hessenberg matrix:

$$\langle\psi_j \mid H_L \mid \psi_k\rangle = \begin{cases} \beta_{jk} \text{ if } j \le k+1 \\ 0 \quad \text{else} \end{cases} ;\ j,k = 0,\ldots,L \qquad (1)$$

(If H is hermitian, then matrix (1) becomes symmetric, i. e. tridiagonal.) The algorithm requires $L+1$ evaluations of $H \mid \psi\rangle$.

The SIL integrator [45] approximates the propagated wave function $\psi(t+\tau)$ by

$$\mid \psi(t+\tau)\rangle = \mathrm{e}^{-\mathrm{i}H_L\tau} \mid \psi(t)\rangle = \sum_{k=0}^{L} a_k^{(L)} \mid \psi_k\rangle \qquad (2)$$

with

$$a_k^{(L)} = \sum_{j=0}^{L} T_{kj}\mathrm{e}^{-\mathrm{i}\lambda_j\tau}\left(\mathbf{T}^{-1}\right)_{j0} . \qquad (3)$$

The λ_j specify the eigenvalues and $\mathbf{T}$ the eigenvector matrix of the small and hence easy to diagonalize upper Hessenberg matrix (1).

The Lanczos recurrence in its standard form is in so far inefficient as the vector ψ_{L+1} as well as the matrix element $\beta_{L+1,L}$ are determined but are never used. A slight modification of the SIL algorithm can circumvent this. As has been suggested by Manthe et al. [64] one may increase the SIL order to $L' = L+1$ by adding a further, approximative, column to the Lanczos matrix. To this end we set $\beta_{L'L'} = \beta_{LL}$, $\beta_{L,L'} = \beta_{L',L}$, and $\beta_{j,L'} = 0$ for $j < L$. The upper Hessenberg matrix is then an $L' \times L'$ matrix, and the summation in (2) and (3) extends to L' rather than L. The wave function propagated with this modified algorithm is correct up to an

order $\tau^{L'}$, while it is only accurate up to an order τ^{L} in the conventional Lanczos scheme.

For the conventional SIL integrator there exists a very convenient estimate for the difference $\Delta\psi$ of the propagated and the exact wave function [45], namely

$$\| \Delta\psi \| \approx \frac{\beta_{10} \ldots \beta_{L+1,L}}{(L+1)!} \tau^{L+1} , \tag{4}$$

which may be used to adjust either the step size τ or the order L. For the modified SIL integrator one could use the same formula but replace L by L'. However, $\beta_{L'+1,L'}$ is unknown, and instead of estimating it we prefer to use (4) as it is. Since for any one-step method such as Lanczos the order of the global discretization error is a power one lower than that of the local error [47], the error estimate therefore controls the global rather than the local error.

Turning again to the conventional Lanczos integrator we note that the error estimate (4) is correct to an order of $L + 1$, yet the true error contains also contributions from higher orders of τ. These contributions depend not only on the sub-diagonal but on all elements of matrix (1). Despite these higher contributions the error formula (4) is remarkably accurate for small step sizes. However, it may grossly overestimate the error when the integrator runs at high orders and thus takes large step sizes.

To arrive at a more reliable error estimate for the (modified) Lanczos integrator we define the error as

$$\| \Delta\psi \| = \| \mathbf{a}^{L'} - \mathbf{a}^{L'-1} \| , \tag{5}$$

where a zero is appended to the shorter of the two vectors, $\mathbf{a}^{L'-1}$. We thus take as error estimate the norm of the difference between the wave functions propagated by the SIL method of order L' and $L' - 1$. We control the accuracy of the propagation by increasing the SIL order L' until the predicted error (5) becomes smaller than the prescribed error tolerance.

The improved error estimate is predominantly determined by the error of the solution obtained with an order of $L' - 1$. Hence the propagated wave function is one order in τ more accurate than the error estimate indicates. This is very much in the spirit to what has been discussed above, namely using (4) for the modified Lanczos integrator as well. Equation (5) seems to be rather costly because it requires after each SIL iteration the diagonalization of matrix (1). However, for large systems the evaluations of $H \mid \psi\rangle$ need so much numerical effort that the effort for the error estimation remains negligible.

As shown in Table 2 the improved error estimate diminished, but did not cure, the Lanczos' efficiency problem. For larger step sizes the efficiency drops by almost a factor of two. We have no explanation for this surprising effect but remark that it may be connected to the MCTDH algorithm, where the propagation matrix $\bar{\mathcal{K}}$ varies from step to step.

References

1. H. Tal-Ezer, R. Kosloff: J. Chem. Phys. **81**, 3967 (1984)
2. C. Leforestier, R. H. Bisseling, C. Cerjan, M. D. Feit, R. Friesner, A. Guldenberg, A. Hammerich, G. Jolicard, W. Karrlein, H.-D. Meyer, N. Lipkin O. Roncero, R. Kosloff: J. Comp. Phys. **94**, 59 (1991)
3. D. Kosloff, R. Kosloff: J. Comp. Phys. **52**, 35 (1983)
4. J. C. Light, I. P. Hamilton, J. V. Lill: J. Chem. Phys. **82**, 1400 (1985)
5. R. Kosloff: J. Phys. Chem. **92**, 2087 (1988)
6. J. C. Light, in Time-Dependent Quantum Molecular Dynamics, ed. by J. Broeckhove, L. Lathouwers (New York, Plenum, 1992), pp. 185–199
7. E. J. Heller: J. Chem. Phys. **62**, 1544 (1975)
8. G. D. Billing: Chem. Phys. **33**, 227 (1978)
9. N. Balakrishnan, G. D. Billing: J. Chem. Phys. **104**, 4005 (1996)
10. M. L. Brewer, J. S. Hulme, D. E. Manolopoulos: J. Chem. Phys. **106**, 4832 (1997)
11. P. A. M. Dirac: Proc. Cambridge Philos. Soc. **26**, 376 (1930)
12. A. D. McLachlan: Mol. Phys. **8**, 39 (1964)
13. P. Jungwirth, R. B. Gerber: J. Chem. Phys. **102**, 6046 (1995)
14. P. Jungwirth, E. Fredj, R. B. Gerber: J. Chem. Phys. **104**, 9332 (1996)
15. J. O. Jung, R. B. Gerber: J. Chem. Phys. **105**, 10332 (1996)
16. H.-D. Meyer, U. Manthe, L. S. Cederbaum: Chem. Phys. Lett. **165**, 73 (1990)
17. U. Manthe, H.-D. Meyer, L. S. Cederbaum: J. Chem. Phys. **97**, 3199 (1992)
18. H.-D. Meyer, U. Manthe, L. S. Cederbaum, in Numerical Grid Methods and their Application to Schrödinger's Equation, ed. by C. Cerjan (Kluwer Academic Publishers, Dordrecht, 1993), pp. 141–152
19. H.-D. Meyer, in Encyclopedia of Computational Chemistry, ed. by P. R. Schleyer (Wiley, New York, 1997), in press
20. U. Manthe, H.-D. Meyer, L. S. Cederbaum: J. Chem. Phys. **97**, 9062 (1992)
21. U. Manthe, A. D. Hammerich: Chem. Phys. Lett. **211**, 7 (1993)
22. A. D. Hammerich, U. Manthe, R. Kosloff, H.-D. Meyer, L. S. Cederbaum: J. Chem. Phys. **101**, 5623 (1994)
23. L. Liu, J.-Y. Fang, H. Guo: J. Chem. Phys. **102**, 2404 (1995)
24. J.-Y. Fang, H. Guo: J. Chem. Phys. **102**, 1944 (1995)
25. A. Capellini, A. P. J. Jansen: J. Chem. Phys. **104**, 3366 (1996)
26. M. Ehara, H.-D. Meyer, L. S. Cederbaum: J. Chem. Phys. **105**, 8865 (1996)
27. A. P. J. Jansen: J. Chem. Phys. **99**, 4055 (1993)
28. A. P. J. Jansen, H. Burghgraef: Surf. Sci. **344**, 149 (1995)
29. J.-Y. Fang, H. Guo: J. Chem. Phys. **101**, 5831 (1994)
30. J.-Y. Fang, H. Guo: Chem. Phys. Lett. **235**, 341 (1995)
31. A. Jäckle, H.-D. Meyer: J. Chem. Phys. **102**, 5605 (1995)
32. G. Worth, H.-D. Meyer, L. S. Cederbaum: J. Chem. Phys. **105**, 4412 (1996)
33. J. Frenkel, Wave Mechanics. Oxford: Clarendon Press 1934
34. R. Kosloff, D. Kosloff: J. Comp. Phys. **63**, 363 (1986)
35. D. Neuhauser, M. Baer: J. Chem. Phys. **90**, 4351 (1989)
36. D. Neuhauser, M. Baer: J. Chem. Phys. **91**, 4651 (1989)
37. T. Seideman, W. H. Miller: J. Chem. Phys. **96**, 4412 (1992)
38. A. Vibok, G. G. Balint-Kurti: J. Chem. Phys. **96**, 7615 (1992)
39. U. V. Riss, H.-D. Meyer: J. Phys. B **26**, 4503 (1993)
40. U. V. Riss, H.-D. Meyer: J. Phys. B **28**, 1475 (1995)
41. U. V. Riss, H.-D. Meyer: J. Chem. Phys. **105**, 1409 (1996)
42. A. Jäckle, H.-D. Meyer: J. Chem. Phys. **104**, 7974 (1996)
43. D. O. Harris, G. G. Engerholm, G. W. Gwinn: J. Chem. Phys. **43**, 1515 (1965)
44. A. S. Dickinson, P. R. Certain: J. Chem. Phys. **49**, 4209 (1968)
45. T. J. Park, J. C. Light: J. Chem. Phys. **85**, 5870 (1986)
46. U. Manthe: J. Chem. Phys. **105**, 6989 (1996)
47. C. W. Gear, Numerical Initial Value Problems in Ordinary Differential Equations. Englewood Cliffs, New Jersey: Prentice-Hall 1971
48. W. E. Arnoldi: Q. Appl. Math. **9**, 17 (1951)
49. Y. Saad: Lin. Alg. Appl. **34**, 269 (1980)
50. R. A. Friesner, L. S. Tuckerman, B. C. Dornblaser, T. V. Russo: J. Sci. Comp. **4**, 327 (1989)
51. W. H. Press, S. A. Teukolsky, W. T. Vetterling, B. P. Flannery, Numerical Recipes. Cambridge: Cambridge University Press 1992
52. U. Manthe, Ph.D. thesis, Universität Heidelberg, 1991
53. V. Engel: Chem. Phys. Lett. **189**, 76 (1992)
54. U. Manthe, private communication
55. M. Shapiro: J. Phys. Chem. **90**, 3644 (1986)
56. P. Botschwina, J. Flesch, W. Meyer: Chem. Phys. **74**, 321 (1983)
57. R. Kosloff, H. Tal-Ezer: Chem. Phys. Lett. **127**, 223 (1986)

58. Y. Amatatsu, K. Morokuma, S. Yabushita: J. Chem. Phys. **94**, 4858 (1991)
59. D. T. Colbert, W. H. Miller: J. Chem. Phys. **96**, 1982 (1992)
60. A. Jäckle, private communication
61. Z. Bačić, J. C. Light: J. Chem. Phys. **85**, 4594 (1986)
62. Z. Bačić, J. C. Light: J. Chem. Phys. **86**, 3065 (1987)
63. S. Liu, Z. Bačić, J. W. Moskowitz, K. E. Schmidt: J. Chem. Phys. **103**, 1829 (1995)
64. U. Manthe, H. Köppel, L. S. Cederbaum: J. Chem. Phys. **95**, 1708 (1991)
65. G. Worth, A. Raab, H.-D. Meyer, L. S. Cederbaum, to be published